DEVELOPMENT OF AN ITERATIVE METHOD FOR LIQUID-PROPELLANT
COMBUSTION CHAMBER INSTABILITY ANALYSIS

A THESIS SUBMITTED TO
THE GRADUATE SCHOOL OF NATURAL AND APPLIED SCIENCES
OF
MIDDLE EAST TECHNICAL UNIVERSITY

BY

KENAN CENGİZ

IN PARTIAL FULFILLMENT OF THE REQUIREMENTS
FOR
THE DEGREE OF MASTER OF SCIENCE
IN
AEROSPACE ENGINEERING

DECEMBER 2010

Approval of the thesis:

DEVELOPMENT OF AN ITERATIVE METHOD FOR LIQUID-PROPELLANT COMBUSTION CHAMBER INSTABILITY ANALYSIS

submitted by **KENAN CENGİZ** in partial fulfillment of the requirements for the degree of **Master of Science in Aerospace Engineering Department, Middle East Technical University** by,

Prof. Dr. Canan ÖZGEN
Dean, Graduate School of **Natural and Applied Sciences**

Prof.Dr. Ozan Tekinalp
Head of Department, **Aerospace Engineering**

Prof. Dr. Yusuf ÖZYÖRÜK
Supervisor, **Aerospace Department**

Examining Committee Members:

Prof. Dr. İsmail H. TUNCER
Aerospace Engineering Dept., METU

Prof. Dr. Yusuf ÖZYÖRÜK
Aerospace Engineering Dept., METU

Prof. Dr. Mehmet ÇALIŞKAN
Mechanical Engineering Dept., METU

Asst.Prof.Dr. Oğuz UZOL
Aerospace Engineering Dept., METU

Assoc.Prof.Dr. D. Funda KURTULUŞ
Aerospace Engineering Dept., METU

Date:

I hereby declare that all information in this document has been obtained and presented in accordance with academic rules and ethical conduct. I also declare that, as required by these rules and conduct, I have fully cited and referenced all material and results that are not original to this work.

Name, Last Name: KENAN CENGİZ

Signature   :

ABSTRACT

DEVELOPMENT OF AN ITERATIVE METHOD FOR LIQUID-PROPELLANT
COMBUSTION CHAMBER INSTABILITY ANALYSIS

Cengiz, Kenan

M.S., Department of Aerospace Engineering

Supervisor   : Prof. Dr. Yusuf ÖZYÖRÜK

December 2010, 58 pages

Controlling unsteady combustion induced gas flow fluctuations and the resultant motor vibrations is a very significant step in rocket motor design. It occurs when the unsteady heat release due to combustion happens to feed the acoustic oscillations of the closed duct forming a feed-back system. The resultant vibrations concerned may even lead to total failure of the rocket system unless analysed and tested thoroughly. This thesis aims developing a linear numerical analysis method for the growth rate of instabilities and possible mode shape of a liquid-propelled chamber geometry. In particular, A 3-D Helmholtz code, utilizing Culick's spatial averaging linear iterative method, is developed to find the form of deformed mode shapes iteratively to obtain possible effects of heat source and impedance boundary conditions. The natural mode shape phase is solved through finite volume discretization and the open-source eigenvalue extractor, ARPACK, and its parallel implementation PARPACK. The iterative method is particularly used for analyzing the geometries with complex shapes and essentially for disturbances of small magnitudes to natural mode shapes. The developed tools are tested via two simple cases, a duct with inactive flame and a Rijke tube, used as validation cases for the code particularly with only boundary contribution and heat contribution respectively. A sample 2-D and 3-D liquid-propelled combustion chamber is also analysed with heat

sources. After comparing with the expected values, it is eventually proved that the method should be only used for determining the mode's instability analysis, as to whether it keeps vibrating or decays. The methodology described can be used as a preliminary design tool for the design of liquid-propellant rocket engine combustors, rapidly revealing only the onset of instabilities.

ÖZ

SIVI YAKITLI ROKET MOTORLARINDA YANMA KARARSIZLIĞININ SAYISAL
ANALİZİ

Cengiz, Kenan

Yüksek Lisans, Havacılık ve Uzay Mühendisliği Bölümü

Tez Yöneticisi   : Prof. Dr. Yusuf ÖZYÖRÜK

Eylül 2010, 58 sayfa

Yanma kararsızlığı ve kontrolü, sıvı ve katı yakıtlı roket motorları tasarımında karşılaşılabilen önemli mühendislik problemlerindendir. Ortamdaki basınç dalgalanmalarıyla yakıtın yanmasından elde edilen ısı enerjisinin birbirini beslemesiyle ortaya çıkar. Bu çalışmada sıvı yakıtlı roket motoru yanma odası kararsızlığı probleminin doğrusal analizini gerçekleştirmek maksadıyla geliştirilmekte olan bir sayısal yöntem anlatılmakta ve basit iki örnek probleme uygulaması sunulmaktadır. Sayısal analiz, ilk aşamada kapalı olduğu varsayılan yanma odasının akustik yapısını belirleyen Helmholtz denkleminin 2 boyutlu sonlu hacimlerle ayrıştırılması sonucu ortaya çıkan doğrusal denklem takımının özgün değerlerinin ve karşılık gelen akustik mod yapılarının ARPACK yazılımı yardımıyla elde edilmesi ile başlar. İzleyen aşamada elde edilen akustik modların ve karşılık gelen dalga numaralarının, gerçek ortamdaki ısı kaynağı ve diğer fiziksel şartlardan kaynaklı etkileşimler ile nasıl değiştiğinin tespiti yapılır. Bunun için karmaşık geometriler için uygulaması nispeten daha kolay olan ve bu yüzden yaygın kullanım bulan Culick'in yinelemeli doğrusal büyüme hızı analizi yöntemi kullanılmaktadır. Geliştirilen bilgisayar programı, ilk aşamada Rijke tüpü problemine uygulanmış ve sonuçlar beklenen doğrultuda çıkmıştır. Sonuçlar göstermektedir ki mod şekli sonuçları güvenilirliği bilinmemekle birlikte, dalga numarasının sanal kısmı modun kararsızlığını belirlemede pekala

kullanılabilir. Hazırlanmış olan bu yöntem, sıvı yakıtlı bir roket motor tasarımının ilk aşamalarında kararsızlıkların ortaya çıkma koşullarını belirlemede hızlı bir araç olarak kullanılabilir.

Anahtar Kelimeler: yanma kararsızlığı, roket motor, termoakustik, rijke tüpü, akustik mod

tüm sabırla bekleyenlere..

ACKNOWLEDGMENTS

TABLE OF CONTENTS

LIST OF TABLES

TABLES

LIST OF FIGURES

FIGURES

xiv

LIST OF SYMBOLS AND ABBREVIATIONS

$()'$ Fluctuations

α Growth rate

$\bar{q_V}$ Volumetric heat release

$\bar{a}$ Mean sound speed

$\bar{p_{CH}}$ Chamber mean pressure

δ_f Flame thickness

γ Specific heat ratio

$\hat{()}$ Time averaged value

$\mathbf{r}$ Displacement vector

ω Frequency

ψ_n n^{th} pure mode's pressure

ρ Density

τ A possible time delay (lag)

C_p, C_v Heat capacities

E_n Euclidean norm of nth mode

f Wave equation boundary condition

h	Wave equation source term
k	Wave number
k_n	n^{th} pure mode's wave number
L	Length
$L1, L2$	Longitudinal modes
l_g	Heater wire mesh position in Rijke tube
n	Flame-flow interaction index
p	Pressure
Q	Heat addition rate
q	Heat addition rate per volume
$R1, R2$	Radial modes
S	Surface area
S_{ref}	Flame area
T	Temperature
t	Time
$T1, T2$	Tangential modes
u	Velocity
V, Ω	Volume
Z	Non-dimensional complex impedance

CHAPTER 1

INTRODUCTION

1.1 BACKGROUND

Rocketry has been developing since the first demonstrative fireworks of Chinese people back in the ninth century. In a search for "elixir of immortality", Chinese alchemists eventually discovered gunpowder, being the precursor of rockets, bombs and guns in any sort. Chinese military then used bamboo tubes to fire mortars with gunpowder as propellant. First rocket was used against Mongols around 1232 AD. Consequently, the technology spread towards west during the Mongolian conquests of Eastern Europe and Middle East. There are historical records that in 13th century the Mongolian Horde used gunpowder-propelled rockets against Magyars in Europe, Arabs and Turks in Middle East [1]. Since then, solid-propellant rockets have been increasingly used in European wars. However, the real achievements were done in the 20th century World Wars. The need of combustion chambers enduring higher pressures and nozzles with more elaborate designs allowing supersonic flows led to the modern rocket technology. Robert Goddard launched the first liquid rocket in 1926 [1]. In the following decades, inter-continental and multi-stage inter-planetary liquid-fuelled rockets were developed, resulting in sound impacts on human history and development. Today, shuttles with a number of liquid-propellant (LOX, liquid hydrogen) rocket engines (Figure 1.1) are able to accomplish demanding space missions, generating totally 36 million hps of power, and 2 million Newtons of thrust each [2].

A liquid rocket simply consists of fuel and oxidizer tanks (e.g. hydrogen and oxygen), combustion chamber, and a nozzle. The basics are quite similar to solid-propellant rockets, using liquid fuels and oxidizer instead. Main design and principles are illustrated in Figure 1.2.
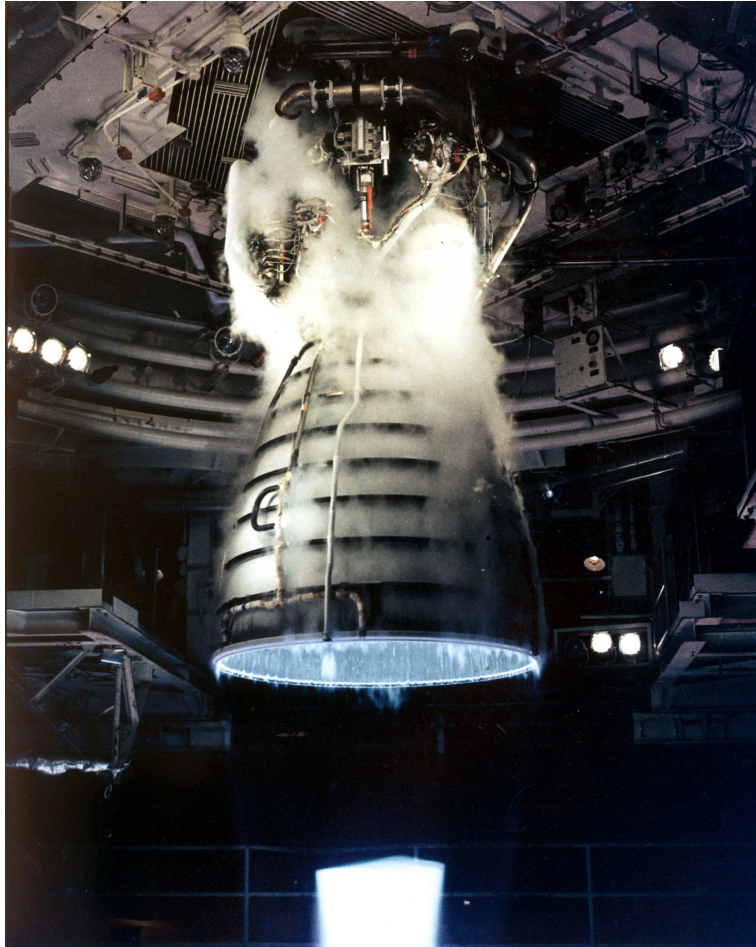
Figure 1.1: Shuttle main engine firing test [2]

Principally in a rocket engine, the chemical energy is converted into kinetic energy, as a high-speed jet aft the nozzle. Combustion chamber is the place where the injection, mixing and ignition of the fuel and oxidizer occurs. Pressure levels are quite high, whereas flow speed is low. In the nozzle, the potential energy of the high pressure flow is converted to high kinetic energy, supplying an incredible momentum to the machine. Aft the nozzle, pressure is usually expands to the ambient pressure (for an ideally expanded nozzle), and the velocity reaches a maximum. In a choked flow, in the diverging part of the nozzle, the flow is always supersonic. The change of pressure and temperature levels through a choked nozzle can be viewed in Figure 1.3.
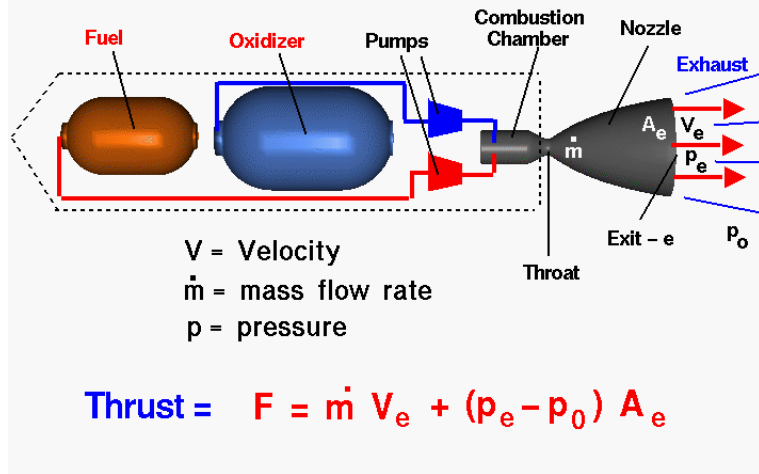
Figure 1.2: A liquid-propelled rocket [2]
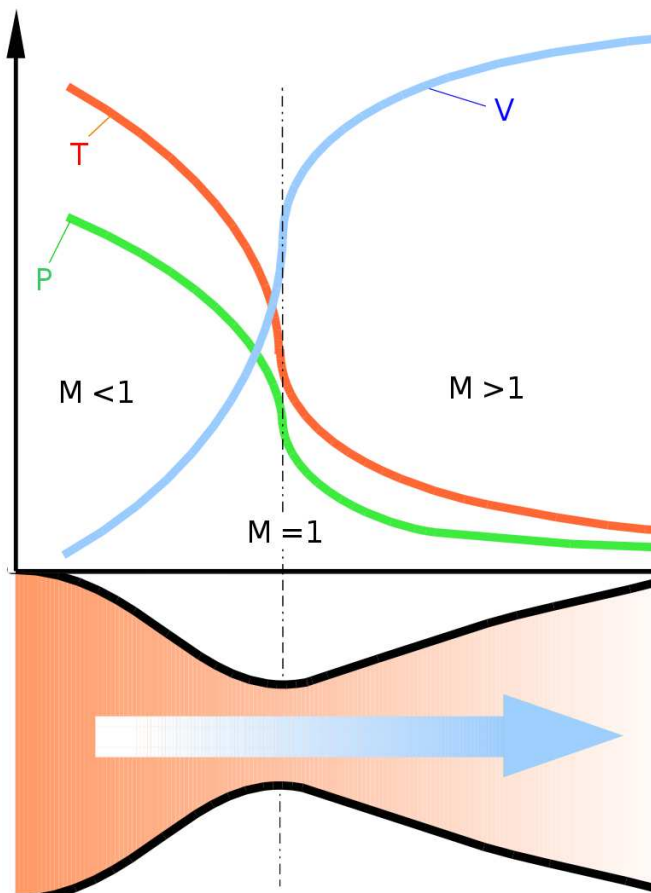
Figure 1.3: Flow variables through the nozzle [2]

1.2 COMBUSTION INSTABILITIES

In modern rocket and gas turbine technology, combustion related instabilities in the chamber have been a challenging issue in design and aft-design period , where the with-coming oscillations must be kept in practical ranges. These oscillations, unless controlled, might impair the efficiency of the combustor, cause unbearable noise to the pilot -if available, cause thermally damage on internal walls, interfere with control devices and injectors, or might even damage the system utterly. Therefore, a thorough analysis and tests must be performed prior to any expensive and painstaking phase of the project. The results should be used to change the design of the chamber geometry, injector design, and if necessary, to include some baffles to modify and absorb vibrations.

In late 1930s, the occurrence of uncontrollable oscillations were first discovered in liquid and solid-propellant rockets. The phenomenon was attributed to high density energy release in a duct with minor losses. The imbalance of energy gains and losses was the fundamental reasoning behind these excitations and sustained oscillations. However, prediction and controlling of instabilities had still been a mystery in most cases. No considerable progress was made until World War II and particularly, the lunar program in 1960s. Since then, Soviet, French and American scientists have been the pioneers in a competitive environment, of the progresses on understanding, analysis and elimination of combustion instabilities, owing to the works such as inter-continental ballistic missiles (ICBMs), space programs and some other launch systems. In space missions, the great efforts and funds spent for development of propulsion systems (e.g. F-1 engine), involving full-scale firing tests, contributed much to the experimental methods and available data for further achievements (see Fig.1.4). Specifically, "Project First" aimed at curing the serious combustion instabilities of the F-1 engine. Approximately 2000 full-scale firing tests were done throughout "Project First". Figure 1.5 demonstrates pressure trace of the F-1 engine, revealing the spontaneous instabilities during a firing test. Gas turbines was not usually problematic as to acoustic instabilities in the early years. The advent of gas turbines in 1940s did not trouble the engineers with challenge of controlling combustion instabilities. However, contamination restrictions imposed in the last decades caused the manufacturers to prefer lean-premixed combustion in gas turbine chambers, leading to serious instabilities difficult to simulate and control. In addition, instabilities in afterburners always stood as a problem to solve.

The most considerable contributions, like always, were brought by the development of computer systems and numerical methods of solution for physical problems. Computational environment enabled us to describe the unsteady problems as finite element discretizations (FEM, FVM, FDM). The most complete solution is given by the DNS or LES. Yet, computational resources still does not meet the requirements of both for full geometry problems. Thus, alternative methods of solution have been suggested, such as Helmholtz solvers, linearized Euler equation solvers, etc. They focus on the most crucial aspects of the unsteady behaviour via appropriate assumptions, and thus reducing the computational costs down to practical levels. However, proper models for mechanisms like fuel injection, droplet formation, vaporization, combustion and baffle/liner damping are still great challenges for the engineers. Hence, numerical simulation is a step to have an idea before costly firing tests of the propulsion system.
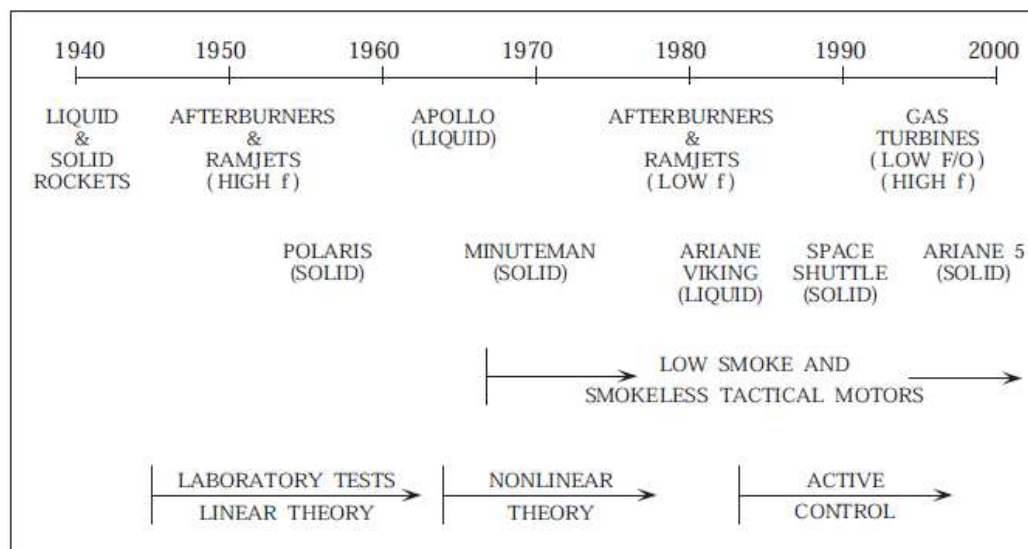
Figure 1.4: A chronology of combustion instabilities [9]

In most cases, combustion itself is stable (in an open-air case for example). What makes the system unstable is the coupling of unsteady combustion with chamber acoustic motions. Basically, the concerned acoustic vibrations in the chamber are driven by the combustion itself when coupled with the acoustic modes of the chamber. For some modes of oscillations, it turns out to be a positively coupling, whence a feedback occurs in-between, resulting in a tendency of the amplitudes to increase. Otherwise, the oscillations diminish before any perception. The phenomenon can be described as a closed-loop feedback system as in Figure 1.6. In a chamber with flow oscillations, the thermal energy is fed into acoustic energy resulting in

5
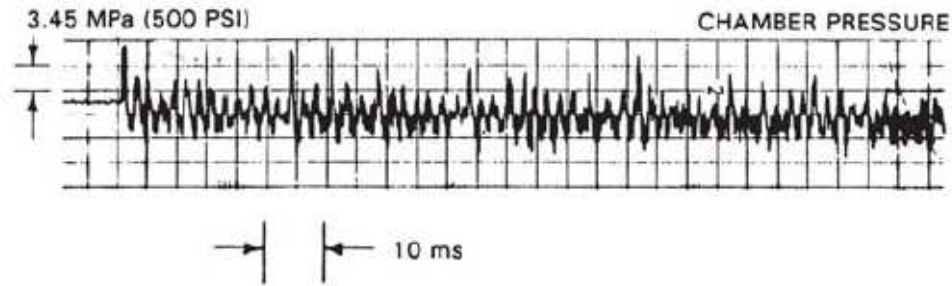
Figure 1.5: Pulses of the injected fuel stream in the F-1 engine [9].

acoustic oscillations with several modes. The oscillating fluid parameters in turn affects the combustion process, resulting in unsteady heat release. This phenomenon is widely called "a thermoacoustic coupling", and when sustained oscillation exist, "thermoacoustic instability". It is first explained by Rayleigh in 1878 [10, 3] by the famous statement which can be deemed as a proverb for thermoacoustics:

"If heat be communicated to, and abstracted from, a mass of air vibrating in a cylinder bounded by a piston, the effect produced will depend upon the phase of the vibration at which the transfer of heat takes place. If heat be given to the air at the moment of greatest condensation, the vibration is encouraged. On the other hand, if heat be given at the moment of greatest rarefaction, or abstracted at the moment of greatest condensation, the vibration is discouraged."

Thus, the Rayleigh criterion may be simply formulated for a period of oscillation

$$\int_T p' q' dt > 0 \tag{1.1}$$

where p' and q' are pressure and heat release oscillations respectively. It is the condition for spontaneously excited acoustic oscillations to appear according to the Rayleigh criterion.

Another indispensable step towards understanding combustion instabilities is the time lag modelling of the coupling, first introduced by Crocco and Cheng in 1956 [4]. They observed that, there is always a time interval between injection of fuel and heat release due to physical procedures like droplet formation, vaporization, wave propagation, etc. This "time lag" delays the response of the acoustic system, generating a phase difference in the temporal behaviour. This way, the oscillations may grow or decay according to the Rayleigh criterion [9, 4], as

6
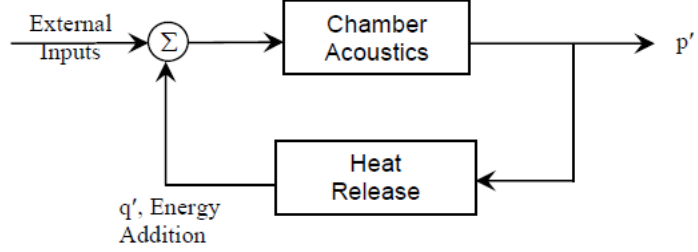
Figure 1.6: Unsteady heat release feeds energy into chamber acoustics.

stated above. Now assume the pressure varies sinusoidally,

$$p' = \hat{p} \sin \omega t \tag{1.2}$$

and assume the energy variation shows up with a constant delay,

$$q' = \hat{q} \sin \omega(t - \tau) \tag{1.3}$$

For low Mach numbers, which is usually the case in a combustion chamber due to very high temperatures (and sound speed, consequently), energy conservation equation gives for a period of oscillation,

$$\Delta E = \frac{\gamma - 1}{p_0 \gamma} \int_V dv \int_t^{t+2\pi/\omega} p'q' = \int_V dv \hat{p}\hat{q} \int_t^{t+2\pi/\omega} \sin \omega t' \sin \omega(t' - \tau)dt' \tag{1.4}$$

$$= \int_V \hat{p}\hat{q}\frac{\pi}{\omega} \cos \omega\tau dv$$

Therefore, Rayleigh criterion tells us that the oscillations are encouraged if $\cos \omega\tau$ is positive; that is, if the heat release is in phase with pressure fluctuations. Simply, the problem can be overcome by keeping the time lag in intervals $\frac{\pi}{2\omega} < \tau < \frac{3\pi}{2\omega}$. However, in realistic situations, the time lag is always dependant on flow variables within complex-geometries, eventually necessitating CFD-CAA (Computational Fluid Dynamics, Computational Aeroacoustics) analysis of the problem together with adequate models for heat release, damping, etc.

1.3 LITERATURE SURVEY

In 1887 Lord Rayleigh in his book [3] first addressed the roles of thermoacoustic coupling phenomenon in closed ducts. He discovered a correlation between the moment of heat addition and the moment of acoustic response. Later in 1956, following the highly experimental

discoveries achieved in World War II, Crocco an Cheng [4] gathered the theory for combustion instabilities in liquid rocket engines and introduced the subject as one of the most challenging topics in combustion and rocket science.

Harrje and Reardon [5] prepared a review on the topic. Later on, several reviews were also published by Culick [6]. Most recently, valuable compilations [7, 8, 9, 10] appeared as extensive materials.

Pieringer and Sattelmayer [45] examined the feasibility of time-domain approach for the solution of linearized governing equations in 3-D liquid rocket engine chamber. Although the equations are linearized for convenience, little assumption was made about the oscillation behaviour.

A frequency-domain wave equation approach, like in the case of this thesis, mostly requires solution of eigenvalue problems. Without any mode-shape assumptions, Nicoud and Benoit, and Nicoud et al. [35, 38] posed problem as quadratic non-linear eigenvalue problems. Hence, the whole problem was formed as a challenging solution of the eigenvalue problem. The care of boundary conditions in the problem was included in a former paper by Lamarque and Poinsot [34]. Solution of the related complex eigenvalue problems are tested in the thesis by Van Leeuwen [36]. The classical Arnoldi method and Jacobi-Davidson method are employed for the solution of thermoacoustic problems to compare the performances. Arnoldi method turned out that it is faster in simple linear problems, whereas Jacobi-Davidson proved to be promising for the most complex non-linear and quadratic eigenvalue problems.

Rubin [31] looked into another aspect of the liquid motor instabilities, POGO instabilities where rocket structural longitudinal mode is coupled with the fluid system, leading to even higher fluid oscillations. The name comes from "pogo stick", because the rocket stretches and compresses like a pogo stick.

The Rijke tube, a tube open both ends with a heater wire mesh on the cross-section to excite longitudinal acoustic oscillations, may be conceived as the simplest case of thermoacoustic instabilities in a duct. Thus, its analysis is definitely invaluable for the general understanding of the instabilities and Rayleigh criterion. Hantschk and Vortmeyer [39] utilized a commercially available CFD software for the solution of Navier-Stokes equation with appropriate boundary conditions in a Rijke tube. They presented nice illustrations of self-excitation in

Rijke tubes, realization of Rayleigh criterion and limit cycles. However, the most comprehensive work about the Rijke tube in both numerical and experimental aspects is perhaps the thesis of Matveev [44]. He developed a theory to model Rijke oscillations and utilized both linear and non-linear heat models with accompanying experimental work. Prediction of the onset of instabilities was fulfilled by a linear analysis, whereas behaviour of the limit cycles was scrutinized by the non-linear modelling together with the mean flow effect. Culick [43] analytically obtained the stability boundaries of the Rijke tube approximately. Vijayakrishnan and Ananthkrishnan in their review [40], summarized the essence and role of Rijke tube in thermoacoustic instabilities, and presented the onset of the instabilities with a simple example. Heckl and Howe [41] developed an analytical solution for the Rijke tube using Green's function approach. Later, Heckl [42] examined several flame transfer functions in frequency domain as to their effect on the stability.

Camporeale et al. [47] proposed a methodology to predict instabilities in a simplified 1-D chamber with passive controlling devices. The passive controlling involves damping using Helmholtz resonators with certain resonant frequencies. Considering two flame models, the damper not only caused the acoustic energy to be dissipated, but also modified the lag between heat release and its acoustic response. Hence, some of the unstable eigenfrequencies forced to be stable with proper use of resonators of the corresponding frequencies.

Another novel method was developed by Cha et al. [48] where a 1-D gas turbine combustor is modelled as a feed-back system, so that classical control theories apply even for complex systems. Heat addition is considered as an input to the closed-loop feed-back system and transfer matrices are formed. Variation of temperature can be modelled by using multi sections through the duct. It is also reported to be straightforward to extend the method to 3-D analysis. Figure 1.7 demonstrates the feed-back loop of the combustion process. H_1 and H_2 stand for the transfer functions between the velocity and heat release U_s, Q.

Sohn et al.[51] utilized a linear acoustic analysis to investigate the damping effects of gas-liquid injectors in liquid rocket combustion chambers. Besides their original use, fuel injection, optimum designs of gas-liquid injectors plays a significant role as damper, eliminating the need of other means of acoustic absorbers such as baffles and liners.

Gudmundsson and Colonius [19] investigated the noise reduction of chevron nozzles in turbofan engines through a linear stability analysis involving a compressible flow solver and eigen-

9
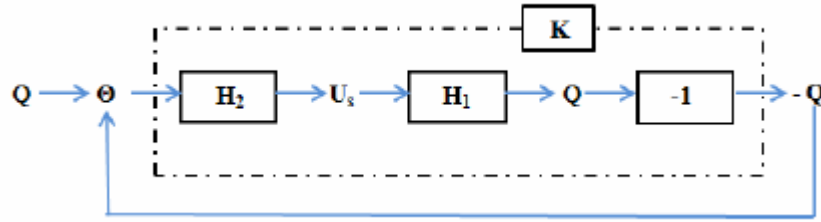
Figure 1.7: Combustion feed-back system model

system solver, ARPACK, in a coupled fashion. The method performed well in simulation of low-frequency noise reduction, which is the primary role of chevron nozzles.

Bogey et al. [52] constructed source terms for linearized Euler's equations taking into account the mean flow effect and vorticity waves. An acoustic analogy is formed to compute the acoustic field once the reference flow field is obtained via LES to construct the source terms. This hybrid method (propagation & generation) can be utilized in instability problems where acoustic-mean flow interactions are significant. Benoit et al., Nicoud and Poinsot [33] also used wave equation together with LES for a reacting flow in a swirled combustor. LES solution of the flow supplies mean temperature field and flame transfer function for the acoustic analysis. Acoustic energy balance methodology served as an evaluation basis for the LES results by realizing the Rayleigh criterion.

Flandro [22] studied the effects of vortex shedding on pressure oscillations in solid-propellant rocket motors. There is a energy flow from the vortex fluctuations to the acoustic field, creating a dipole or quadrapole mechanism. Figure 1.8 shows the analysis model for vortex-generated sound. It is found that the location and orientation of vortical structures with respect to acoustic waves is quite decisive on damping or driving characteristic of vorticity waves. In a solid-propellant rocket, the rotational effects significantly modifies the longitudinal modes of oscillation due to slip condition on burning surface. Moreover, the radial modes are also disturbed because of normal vertical oscillations caused by vortical structures. Flandro, in a following work [23] constructed an approach for the inclusion of rotational effects in the "Standart Stability Prediction Program (SSP)". It was an 3-D improvement to the Culick's one-dimensional flow-turning correction, where radial velocity corrections on the burning surface is also included. The outcome revealed that this extra driving effect makes the solid rocket less stable than previously predicted in SSP.
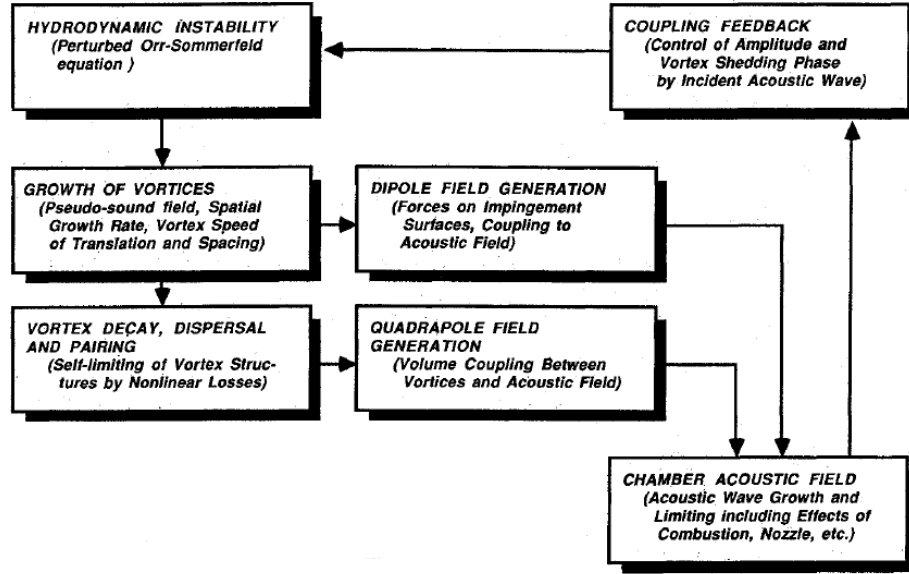
Figure 1.8: Hydrodynamic-acoustic interactions [22].

French et al.[24, 26, 27, 28, 29, 30] came up with many improvements and automations for the solid rocket stability programs SSP & SPP (Standard Stability Program & Solid Propellant Performance). The works mostly put effort on tangential modes of vibration where previously difficulties existed with accuracy aspects. To obtain the transverse mode shapes accurately, they implemented Green's Function Discretization (GFD) [24, 25] requiring less nodes per wave length. A novel technique is employed for the eigenvalue extraction of the discretized equations. A range of frequencies are solved with an arbitrary source term on the right-hand side of the discretized form of the eigenvalue problem [24, 26]

$$M_{ij}\phi_j = e_i \tag{1.5}$$

where e_i is the small perturbation to the system acting as a source. As the desired frequency range is swept with small intervals, the resonant modes peak in amplitude as shown in Figure 1.9. This method proved to be faster than standard techniques when a wide range of frequencies is in question.

1.4 OBJECTIVES

The objective of this thesis is to develop a 3-D homogeneous Helmholtz solver and iterative combustion instability code for finding acoustic mode shapes and complex wavenumbers in

11
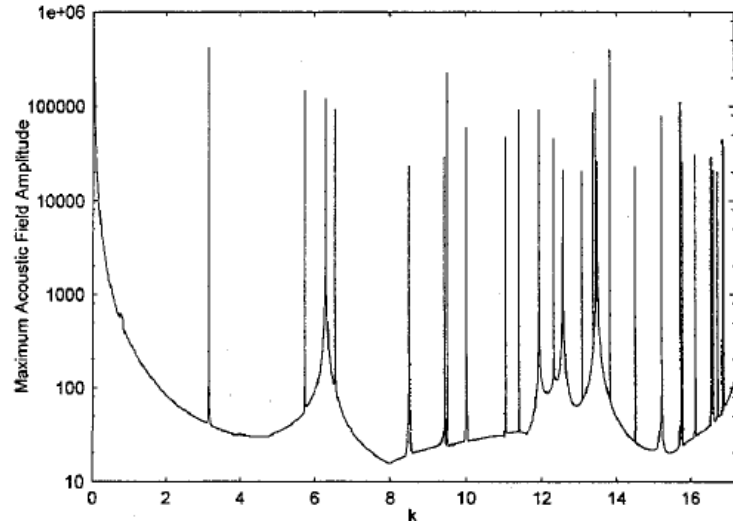
Figure 1.9: The French method for eigen-problem solution [24]

3-D combustion chambers. The iterative combustion instability code is a linear analysis tool, which iteratively imposes inhomogeneous terms on the homogeneous Helmholtz equation (sources such as heat source; and inhomogeneous boundary conditions, such as an impedance condition), consequently supplying the actual mode shape and complex wavenumber to determine the growth and damping characteristics of the oscillations as a first step towards stability analysis of the combustion chambers. In Chapter 2, the theory behind the developed code *HELM2D/3D* and *YAKAR* is explained thoroughly. Eigenvalue problem solution process is also explained both for serial and parallel implementations. In Chapter 3, a duct with impedance boundary condition and inactive flame is examined. In Chapter 4, the well-known Rijke tube case is considered as to the vibration behaviour of the fundamental acoustic mode. Chapter 5 is intended to simulate a fictional liquid-propelled rocket combustion chamber in choked condition, both for 2-D and 3-D cases. Finally, Chapter 6 summarizes what have been studied and concludes the results of the various cases.

CHAPTER 2

EQUATIONS OF LINEAR COMBUSTION INSTABILITIES

The method described in this chapter will be for linear combustion analysis in a chamber. Methods used for analysis of nonlinear behaviour mostly have roots in this linear analysis developed in early works of Culick [21, 20]. The analysis is mainly based on the assumption of small deviations from a homogeneous problem, making use of Green's function theorem.

2.1 THE WAVE EQUATION

In order to obtain inhomogeneous wave equation, one must start with inhomogeneous set of flow equations. Because viscous effects are most of the time negligible in acoustic processes having small perturbations of flow variables, Euler equations are best to start with. The following assumptions would guide us in the conservation equations to be used [10].

- C_p, C_v and γ are constants

- p_0, u_0, ρ_0 are uniform throughout the chamber. For a liquid-propellant engine, it is not a problem to assume uniform flow throughout the chamber where high pressures and temperatures exist, whereas Mach numbers are low (except for the nozzle). However it is not very realistic to assume T_0 constant in a rocket combustor.

- Steady flow and waves.

- Only a heat source will be taken into account, being the heat release of combusting fuel.

- Fluctuations of u, p, T, ρ and q are small enough.

therefore, the linearized Euler equations can be derived (see Appendix A):

$$\frac{\partial \rho'}{\partial t} + \nabla \cdot (\rho_0 \vec{V'}) \;=\; 0 \tag{2.1}$$

$$\frac{\partial \vec{V'}}{\partial t} + \frac{1}{\rho_0} \nabla p' \;=\; 0 \tag{2.2}$$

$$\frac{\partial p'}{\partial t} + \gamma p_0 \nabla \cdot \vec{V'} \;=\; (\gamma - 1) q' \tag{2.3}$$

where q' is the oscillatory heat source. Now, subtracting $\frac{\partial}{\partial t}$(Eq.2.3) from $\gamma p_0 \nabla \cdot$(Eq.2.2), we obtain the wave equation

$$\frac{\gamma p_0}{\rho_0} \nabla^2 p' - \frac{\partial^2 p'}{\partial t^2} \;=\; -(\gamma - 1)\frac{\partial q'}{\partial t}$$

which becomes,

$$\nabla^2 p' - \frac{1}{\bar{a}^2}\frac{\partial^2 p'}{\partial t^2} = h \tag{2.4a}$$

$$\mathbf{n} \cdot \nabla p' = -f \tag{2.4b}$$

where $\bar{a}^2 = \frac{\gamma p_0}{\rho_0}$ is the mean sound speed, and f is a possible boundary condition revealing reflective behaviour of the internal boundaries of the chamber. $h = -\frac{\gamma - 1}{\bar{a}^2}\frac{\partial q'}{\partial t}$ is the source term consisting purely of heat release of combusting fuel.

Equations (2.4) are the equations to be solved throughout the chamber for the steady waves. However, determining the pressure oscillations would not yield the stability behaviour by itself. We will need further interpretations for the phenomenon.

2.2 EXPANSION IN MODES AND SOLUTION BY ITERATION

Now that wave equation is derived, the procedure explained in detail in [9] may be developed. For the solution of pressure, Green's function expression will be utilized together with some other expressions.

Because the fluctuations are assumed small for an acoustic process in the chamber, they can be taken as small harmonic oscillations around a mean:

14

$$p' = \hat{p}e^{-i\bar{a}kt} \quad ; \quad q' = \hat{q}e^{-i\bar{a}kt} \tag{2.5}$$

where $\bar{a}$ is the mean sound speed and k is the complex wave number unknown initially,

$$k = \frac{1}{\bar{a}}(\omega + i\alpha) \tag{2.6}$$

Here, α is known as the growth rate. It is obvious that a positive α means the wave is growing in amplitude, $p' \sim e^{\alpha t}$, whereas a negative value causes the oscillations to diminish. In classical acoustics, it is known that $h = f = 0$ inherently; hence the wave turns out to be stationary with no imaginary part of the wave number. Moreover, $\alpha << \omega$ would be a reasonable assumption for combustion processes where the waves are decaying or growing slowly. It is also a reasonable assumption that sources are small perturbations of the classical field with no sources. Therefore, we can write,

$$h = \kappa\hat{h}e^{-i\bar{a}kt} \quad ; \quad f = \kappa\hat{f}e^{-i\bar{a}kt} \tag{2.7}$$

where κ is a small parameter included to guarantee the smallness of h and f. Hence the equation (2.5) yields the inhomogeneous Helmholtz equation

$$\nabla^2\hat{p} + k^2\hat{p} = \kappa\hat{h} \tag{2.8a}$$

$$\hat{\mathbf{n}} \cdot \nabla\hat{p} = -\kappa\hat{f} \tag{2.8b}$$

The best method here to solve the linear problem is the use of Green function to convert the differential equation into integral equation [9]. Thereby, an iterative method may be constructed to obtain the complex wavenumber explicitly.

2.2.1 Green's Function, Modal Expansion and Spatial Averaging

Now, define a Green's function with homogeneous boundary condition,

$$\nabla^2 G(\mathbf{r}|\mathbf{r_0}) + k^2 G(\mathbf{r}|\mathbf{r_0}) = \delta(\mathbf{r}|\mathbf{r_0}) \tag{2.9a}$$

$$\hat{\mathbf{n}} \cdot \nabla G(\mathbf{r}|\mathbf{r_0}) = 0 \tag{2.9b}$$

where $G(\mathbf{r}|\mathbf{r_0})$ is the Green's function of the wave observed at $\mathbf{r}$ due to the source at $\mathbf{r_0}$. Multiply (2.8a) by $G(\mathbf{r}|\mathbf{r_0})$; (2.9a) by $\hat{p}(r)$, subtract the results and integrate over the volume

15

in question to obtain

$$\iiint_V G(\mathbf{r}|\mathbf{r_0})\nabla^2 \hat{p}(\mathbf{r}) - \hat{p}(\mathbf{r})\nabla^2 G(\mathbf{r}|\mathbf{r_0})]dV \tag{2.10}$$

$$= \kappa \iiint_V G(\mathbf{r}|\mathbf{r_0})\hat{h}(\mathbf{r})dV - \iiint_V \hat{p}(\mathbf{r})\delta(\mathbf{r} - \mathbf{r_0})dV$$

Utilizing Green's theorem for the first integral, and sifting property of the delta function is applied to the second integral on the right-hand side:

$$\oiint_S [G(\mathbf{r}|\mathbf{r_0})\nabla \hat{p}(\mathbf{r}) - \hat{p}(\mathbf{r})\nabla G(\mathbf{r}|\mathbf{r_0})] \cdot \hat{\mathbf{n}}dS = \kappa \iiint_V G(\mathbf{r}|\mathbf{r_0})\hat{h}(\mathbf{r})dV - \hat{p}(\mathbf{r_0}) \tag{2.11}$$

Applying the boundary conditions (2.8b) and (2.9b) gives,

$$\hat{p}(\mathbf{r_0}) = \kappa \left\{ \iiint_V G(\mathbf{r}|\mathbf{r_0})\hat{h}(\mathbf{r})dV + \oiint_S G(\mathbf{r_s}|\mathbf{r_0})\hat{f}(\mathbf{r_s})dS \right\} \tag{2.12}$$

where the subscript "s" ensures that it lies on the boundary surface.

Physically, the wave observed at $\mathbf{r}$ due to a point source at $\mathbf{r_0}$ has the same effect as for the wave observed at $\mathbf{r_0}$ subject to a point source at $\mathbf{r}$. Hence, the Green's function for the wave operator possesses symmetry property

$$G(\mathbf{r}|\mathbf{r_0}) = G(\mathbf{r_0}|\mathbf{r}) \tag{2.13}$$

Then the equation (2.12) becomes,

$$\hat{p}(\mathbf{r}) = \kappa \left\{ \iiint_V G(\mathbf{r}|\mathbf{r_0})\hat{h}(\mathbf{r_0})dV_0 + \oiint_S G(\mathbf{r}|\mathbf{r_{0_s}})\hat{f}(\mathbf{r_{0_s}})dS_0 \right\} \tag{2.14}$$

Now on, it comes to determine the Green's function. The most convenient way to express it for the case is expansion in normal modes of the chamber, that is, eigenfunctions $\psi(\mathbf{r})$ of classical acoustics problem (see section2.3).

$$G(\mathbf{r}|\mathbf{r_0}) = \sum_{n=0}^{\infty} A_n \psi_n(\mathbf{r}) \tag{2.15}$$

The natural modes ψ_n satisfy the homogeneous Helmholtz equation (2.24) and are orthogonal functions,

$$\iiint_V \psi_m(\mathbf{r})\psi_n(\mathbf{r})dV = E_n^2 \delta_{mn} \tag{2.16}$$

16

Substituting (2.15) in (2.9), then multiplying by $\psi_m(\mathbf{r})$ gives after integration over the volume,

$$\iiint_V \psi_m \sum_{n=0}^{\infty} A_n \nabla^2 \psi_n dV + k^2 \iiint_V \psi_m \sum_{n=0}^{\infty} A_n \psi_n dV = \iiint_V \psi_m(\mathbf{r})\delta(\mathbf{r} - \mathbf{r_0})dV$$

A_n can be determined by using (2.24), (2.16) and sifting property of delta function,

$$A_n = \frac{\psi_n(\mathbf{r_0})}{k^2 - k_n^2} \tag{2.17}$$

Eventually, the modal expansion of the Green's function appears as

$$G(\mathbf{r}|\mathbf{r_0}) = \sum_{n=0}^{\infty} \frac{\psi_n(\mathbf{r})\psi_n(\mathbf{r_0})}{E_n^2(k_n^2 - k^2)} \tag{2.18}$$

Substitution of the expansion in (2.14) leads to the expansion of the pressure field

$$\hat{p}(\mathbf{r}) = \kappa \sum_{n=0}^{\infty} \frac{\psi_n(\mathbf{r})}{E_n^2(k^2 - k_n^2)} \left\{ \iiint_V \psi_n(\mathbf{r_0})\hat{h}(\mathbf{r_0})dV_0 + \oiint_S \psi_n(\mathbf{r_{0_s}})\hat{f}(\mathbf{r_{0_s}})dS_0 \right\} \tag{2.19}$$

The pressure field should approach the unperturbed mode shape ψ_N, while κ is approaching zero. To provide grounds for this condition, isolation of the Nth term from the pressure expansion yields

$$\hat{p}(\mathbf{r}) = \psi_N(\mathbf{r})\frac{\kappa}{E_N^2(k^2 - k_N^2)} \left\{ \iiint_V \psi_N(\mathbf{r_0})\hat{h}(\mathbf{r_0})dV_0 + \oiint_S \psi_N(\mathbf{r_{0_s}})\hat{f}(\mathbf{r_{0_s}})dS_0 \right\} \tag{2.20}$$

$$+ \kappa \sum_{n=0}^{\infty}{}' \frac{\psi_n(\mathbf{r})}{E_n^2(k^2 - k_n^2)} \left\{ \iiint_V \psi_n(\mathbf{r_0})\hat{h}(\mathbf{r_0})dV_0 + \oiint_S \psi_n(\mathbf{r_{0_s}})\hat{f}(\mathbf{r_{0_s}})dS_0 \right\}$$

The prime sign means the $n = N$th term is missing among the terms of summation. To provide $\hat{p} \xrightarrow{\kappa \to 0} \psi_N$, the term multiplying ψ_N must be unity. Hence, the formula for the perturbed wavenumber can be obtained as

$$k^2 = k_N^2 + \frac{\kappa}{E_N^2} \left\{ \iiint_V \psi_N(\mathbf{r_0})\hat{h}(\mathbf{r_0})dV_0 + \oiint_S \psi_N(\mathbf{r_{0_s}})\hat{f}(\mathbf{r_{0_s}})dS_0 \right\} \tag{2.21}$$

And the pressure expansion is simply

$$\hat{p}(\mathbf{r}) = \psi_N(\mathbf{r}) + \kappa \sum_{n=0}^{\infty}{}' \frac{\psi_n(\mathbf{r})}{E_n^2(k^2 - k_n^2)} \left\{ \iiint_V \psi_n(\mathbf{r_0})\hat{h}(\mathbf{r_0})dV_0 + \oiint_S \psi_n(\mathbf{r_{0_s}})\hat{f}(\mathbf{r_{0_s}})dS_0 \right\} \tag{2.22}$$

(2.21) may also be derived more directly. Multiply (2.4) by ψ_N, integrate over the volume, together with (2.24) after manipulations to obtain

$$k^2 = k_N^2 + \frac{\kappa}{\iiint_V \psi_N \hat{p}dV} \left\{ \iiint_V \psi_N(\mathbf{r_0})\hat{h}(\mathbf{r_0})dV_0 + \oiint_S \psi_N(\mathbf{r_{0_s}})\hat{f}(\mathbf{r_{0_s}})dS_0 \right\} \tag{2.23}$$

17

It can be shown from (2.22) that the integral on the denominator of (2.23) is equal to E_N^2 if the series in (2.22) converges. However, the validity of this equation is subject to discussion [10]. Hence, the former is adopted.

The equations gathered (2.22),(2.21) are means to build a solution for the complex wavenumber, k. However, the wavenumber is always dependant on pressure, as $\hat{h}$ and $\hat{f}$ are mostly dependant on pressure. Therefore, an iterative method is the primary choice for solution. Because the deviation from the unperturbed mode, k_N, is taken to be small by the order of κ an iterative procedure should be legitimate.

2.2.2 Iterative method

It can be proved that wavenumber and pressure distribution correct to the order m in κ requires those of order $m - 1$. Hence, a successive iteration is straightforward.

Now, initialize $\hat{p}$ with $\kappa = 0$,

$$\hat{p}^{(0)} = \psi_N$$

Substitution into (2.23) gives k^2 correct to first order in κ, $(k^2)^{(1)}$. Similarly, $\hat{p}$ first-order accurate in κ requires $\hat{p}$ and k^2 to zeroth-order accurate values, $\hat{p}^{(0)} = \psi_N$ and $(k^2)^{(0)} = k_N^2$. This way, an iteration can be performed until both values converge.

Up to this point, the theory behind the iterative method is explained. To summarize the procedure to be followed, a schema of the pathway towards the instabilty analysis is shown in Fig.2.1. The principal result to be obtained is the information whether the mode will vibrate or not, by solely checking whether the imaginary part of the perturbed wavenumber is positive or negative.

2.3 HARD-WALL NATURAL MODES

Natural mode shape is the modal solution of the homogeneous Helmholtz equation of a closed chamber, giving possible oscillation spectra of any perturbation in the chamber. It depends purely on the geometry of the closed section in question. It can be discretized simply by utilizing a finite element method throughout the closed chamber, then posing it as an eigenvalue
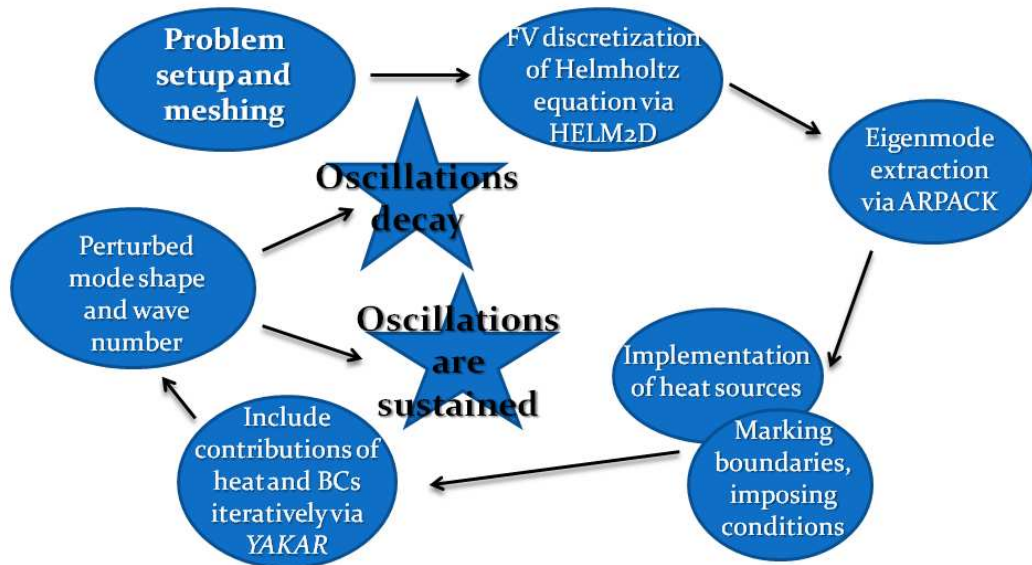
Figure 2.1: Waypoints for the linear combustion stability analysis

problem. Homogeneous Helmholtz equation

$$\nabla^2 \psi_n + k_n^2 \psi_n = 0 \tag{2.24a}$$

$$\hat{\mathbf{n}} \cdot \nabla \psi_n = 0 \tag{2.24b}$$

is the equation to be solved with homogeneous boundary condition the find the natural modes of the combustion chamber.

2.3.1   FINITE VOLUME DISCRETIZATION

A 2nd order 2-D finite volume discretization code, and a 3-D version, *HELM2D* & *HELM3D* are developed. A higher order finite difference would seem attractive at a first glance, but the ease of grid generation even for the most complex geometries tempted to choose finite volume method. Therefore an accuracy analysis will have to be performed for selection of the correct fineness of the mesh. The code is able to form the solution matrix efficiently and swiftly, always working with sparse forms in complex domain.

The homogeneous Helmholtz equation (2.24) can be expressed in integral form as

$$\oint \vec{\nabla}\psi_n \cdot \vec{ds} + \int_\Omega k_n\psi_n d\Omega = 0 \tag{2.25}$$

It is now obviously described throughout a volume. Provided the equation is conformed to finite tetrahedral volumes of a 3-D domain,

$$\sum_{s=1}^{4} \vec{\nabla}\psi_{n,i,s} \cdot \vec{\Delta s_i} + k_n\Omega_i\psi_{n,i} = 0 \tag{2.26}$$

where the subscript n defines eigenvalue indices, i is the cell number index, and s is for the surfaces of the tetrahedral cell. A cell-based finite volume scheme is employed for this discretization. On boundary cells, necessary care is taken to diminish in-flux and equate the values on ghost cells.

2.3.2   EIGENVALUE PROBLEM SOLUTION

The discretized form of the finite volume solution is constructed as an eigenvalue problem. The open-source software ARPACK and PARPACK are utilized for the iterative solution of the large-scale eigenvalue problem to be solved for the mode shape [12, 13, 14, 17]. PARPACK [15] is the parallelized version of ARPACK, both of which are based on an algorithmic variant of Arnoldi process called Implicitly Restarted Arnoldi Method (IRAM). Some remarkable works are available in the literature which utilize ARPACK [19, 24, 29, 32, 34]. However, the fact that it only allows limited number of eigenvalues to be extracted renders our work a bit of cumbersome. In the equations (2.21), (2.22) it is obvious that theoretically infinite; practically all eigenvalues are needed for realistic convergence. A finite number of eigenmodes would solely be an approximate approach, as the method itself is. In a discrete system, a limited number of mode shapes would be possible to capture after all.

Particularly for the 3-D problem, essentially PARPACK should be employed. For that purpose, a driver routine that can handle partitioning, parallel matrix-vector multiplication and data gathering have been developed. The driver routine calls MPI blocking message passing routines for communication(MPI_Send, MPI_Receive, MPI_Bcast, MPI_Gatterv). "MPI_Send, MPI_Receive" is used to distribute the work among the processes equally. The multiplication is conveniently performed via "MPI_Reduce_Scatter" routine with "MPI_SUM" operator. The results are then collected on the master process via "MPI_Gatterv". The designed way of sharing of work and matrix multiplication can be simply illustrated through

Figure 2.2 for a world of 3 processes. The routine also accomplishes the necessary tasks and communication in sparse sense, reducing the amount of memory required and CPU clock.
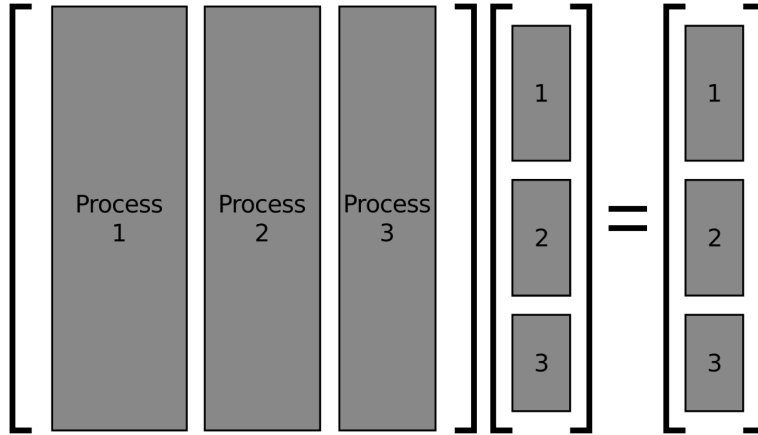
Figure 2.2: Parallel matrix-vector multiplication

2.3.3   VALIDATION OF MODE SHAPE ANALYSIS

The eigenfunction extraction algorithm must be validated before any progress in further analysis. A block-shape domain is chosen for validation, for which analytic solution of the Helmholtz equation is simply available through harmonic solutions together with the dispersion relation,

$$\psi_{lmn} = A e^{i\frac{l\pi}{a}x} e^{i\frac{m\pi}{b}y} e^{i\frac{n\pi}{c}z} \tag{2.27a}$$

$$k_{lmn} = \left(\frac{l\pi}{a}\right)^2 + \left(\frac{m\pi}{b}\right)^2 + \left(\frac{n\pi}{c}\right)^2 \tag{2.27b}$$

Here, a, b and c are lengths of the sides on x, y and z direction respectively. In the figure 2.3, a comparison of the analytical solution and discrete solution is depicted. The numerical solution is normalized with maximum magnitude available, in order to eliminate calculation of A. It can be observed that the results do not match adequately (Figure 2.4). Most importantly, the wavenumber is deviated from the expected value. Hence, finer meshes and higher orders of discretizations may be needed. However, after some trials with million cells, it is concluded that any improvement on fineness wouldn't help, because of the implicit limit imposed by the 2th order finite volume discretization. Hopefully, a finite element discretization

with quadratic interpolation functions and natural boundary condition imposition will eliminate the deviations and numerical oscillations. For the time being, it is solely considered as a future work. Therefore, except for the rough estimations for the rocket chamber in Chapter 5, 2-D simulation is adopted.
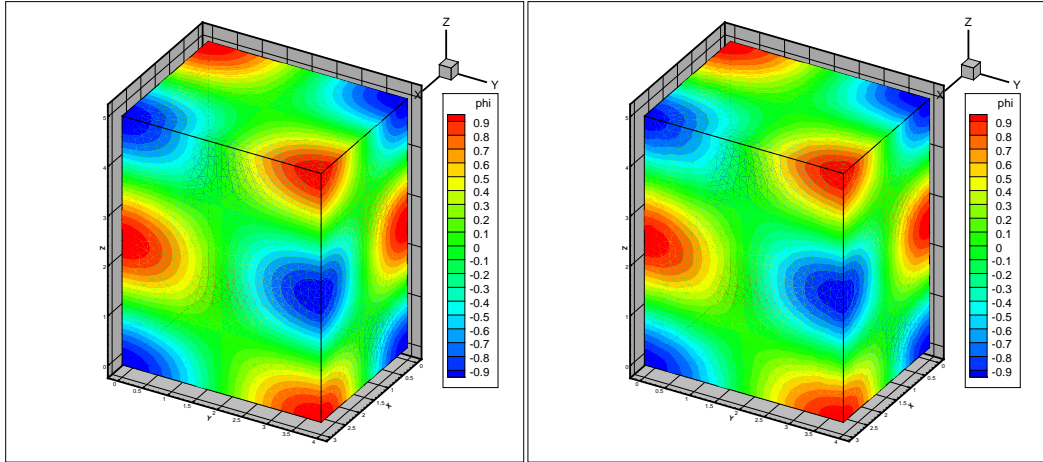
Figure 2.3: $(1, 1, 3)^{th}$ mode shape of the analytical solution (left) and of the numerical solution (right)

Owing to the fact that choice of adequate number of cells for acceptable accuracy is affordable and that boundary condition have been imposed flawlessly, finite volume natural mode extractor works well in 2-D discretization. Longitudinal and complex mode shape of a rectangular domain of length $1\,m$ is examined (Figure 2.5, 2.6). The mesh resolution is approximately 30 longitudinal intervals per wave length for the tenth longitudinal mode, and the same number of intervals per wave length for the first transverse mode. Clearly, the modes shown are resolved accurately. However, it's for sure that higher modes will fail beyond a limit, all of which must be avoided for the sake of reliable analysis.

2.4 SOURCE TERM

As mentioned earlier, only heat source term on the Euler equations is considered in this study. Physically, it stands for a heat addition due to combustion of fuel with neglected mass and momentum. The region of heat release can be modelled as a thin flame enclosed by the cross-section of the duct at a location in the axis. Therefore, a 1-D heat release model can be
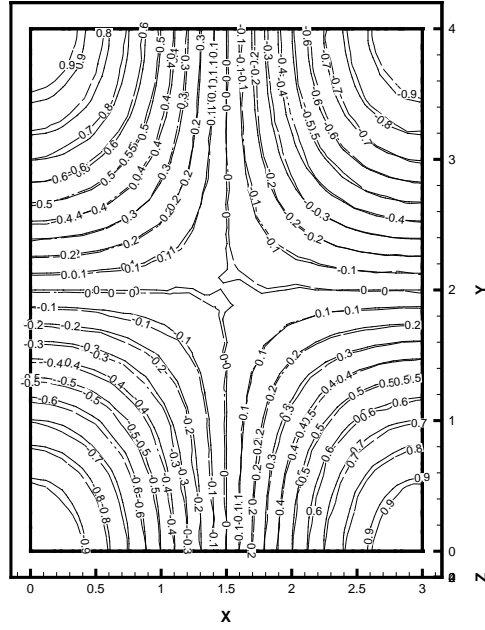
Figure 2.4: Comparison of $(1, 1, 3)^{th}$ mode shape of the analytical solution (solid line) and of the numerical solution (dashed line) at $z = 2.5$ plane

developed making use of the time-lag model by Crocco [4]. According to his general time-lag description, the heat release at a point is dependant on pressure and velocity at that point at a former time. Moreover, whatever the physical process might be, pressure and velocity contributions must be formed as a linear combination of both, for solely linear behaviour is accounted in the analysis. Then the heat source becomes

$$\dot{q}' = Ap'(x, t - \tau_p) + Bu'(x, t - \tau_u) \tag{2.28}$$

or equivalently in frequency domain

$$\hat{\dot{q}}(x, \omega) = A\hat{p}(x, \omega)e^{-i\omega\tau_p} + B\hat{u}(x, \omega)e^{-i\omega\tau_u} \tag{2.29}$$

Depending on the combustion dynamics, specific coefficients and lags may be chosen. The coefficients and lags are normally distributed fields hardly deduced from LES and experimental results [52, 33]. Generally, however, combustion in a rocket motor is taken to be dependant on pressure mostly, whereas for a Rijke tube, heat release is determined by velocity at most, controlling the rate of heat transfer through the hot wire. Specific choices will be made in the cases discussed in the next chapters.

23
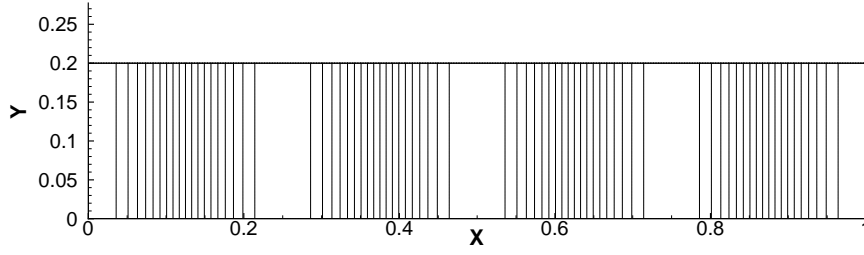
Figure 2.5: (4,0) natural mode shape (lines: analytical solution $k = 3.14159$ rad/m; dots: numerical solution $k = 3.14158$ rad/m.)
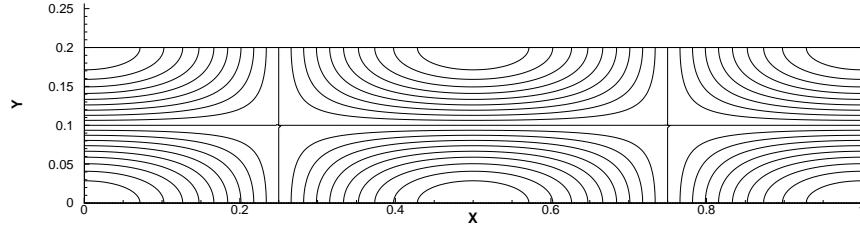
Figure 2.6: (2,1) natural mode shape (lines: analytical solution $k = 16.9180$ rad/m; dots: numerical solution $k = 16.9163$ rad/m.)

2.5 BOUNDARY CONDITIONS

As stated earlier in (2.8), $\hat{f}$ is a term included on boundaries, imposing the influence of boundary conditions on the wave system. Provided it is taken to be zero, the boundary in question will spontaneously be a hard wall, without any flow in perpendicular direction. However, if an impedance condition is to be imposed on the boundary, the impedance definition must be considered first

$$Z = \frac{\hat{p}}{\rho_0 \bar{a} \hat{\mathbf{u}} \cdot \hat{\mathbf{n}}} \tag{2.30}$$

From momentum equation (2.1) in frequency domain we have

$$\hat{u} = \frac{\nabla \hat{p}}{ik\bar{a}} \tag{2.31}$$

Then, one can get a formula for $\hat{f}$

$$\hat{f} = -\frac{ik\hat{p}}{Z} \tag{2.32}$$

Any impedance condition Z can be used to simulate a boundary's behaviour. Impedance condition of a damping device or nozzle mostly depends on frequency and flow parameters. Special treatment must be done for open atmosphere (infinitely large medium) condition $\hat{p} = 0$,

24

though. Clearly, $\hat{f}$ must have such a value that all pressure oscillation values in cells on the boundary are forced to be zero. This can be achieved simply by equating pressure to zero in equation (2.22), resulting in a system of linear equations throughout the boundary cells with $\hat{f}$ as unknowns. This procedure is crucial on every step of the iterations. Thus, a linear system solver from LAPACK [18] package is simply employed on each iteration step.

2.6 NUMERICAL ASPECTS

In the 2-D analysis explained, since rank of matrices -being equal to number of cells- are not extremely large most of the time, the serial version of ARPACK suffices on Opteron machines with 6 GB of memory (the "akbaba" cluster in METU/AEE). Extraction of modes never took more than tens of minutes. Despite ARPACK's iterative nature, the memory is a severe computational requirement for 3-D cases due to large matrices, being unable to compute about matrices of 150000 rank or more. Moreover, for such matrices the Arnoldi vectors generated and Arnoldi iterations in ARPACK increase in number, causing the simulation to take longer computational time. The parallel implementation PARPACK is a good solution for such cases, sharing both memory and work among the computers of a cluster. For example, a matrix with 1.7 million of rank can be solved for few eigenvalues at around 15 hours on 15 processes. As to the simulation with the iterative method YAKAR2D, depending on the complexity of heat and boundary condition terms, the iterations converged from 4-5 iterations up to 30-40 iterations, taking tens of minutes at most. The 3-D case took more iterations and time, up to 1-2 hours depending on the conditions. In addition, although the iterative code is not developed to work in parallel, a "quasi-parallel" means of computation helped much in simulations, in which different machines were assigned independently to simulate for different modes at the same time without any need of communication. It should be a better way to share work among the machines.

Up to here, the necessary tools and methods for the analysis of linear combustion instability in ducts has been constructed. In the following chapters, validation, analysis and experimentation of various cases of ducts will be performed.

CHAPTER 3

A TEST CASE WITHOUT FLAME

In this chapter, a simple test case with inactive flame and an impedance boundary condition on one wall is considered. Several tests are performed to comprehend the behaviour of the iterative solution method as various parameters of solution are changed.

3.1 VALIDATION OF NATURAL MODES

Before studying any cases with perturbation, the natural mode shapes must be validated properly. In this chapter a test case, which is also examined by Nicoud et al. [38], is analysed. It is a simple rectangular 2-D duct with dimensions $L = 1 \times 0.2$ m. The domain is divided into uniform triangular cells in an aim to reduce numerical errors. As discussed in Chapter 2, about 60 cells per wave length ($0.0033m$ of intervals in longitudinal direction) will be safe to use up to 10th longitudinal mode and 2nd transverse mode. That makes a total of 36000 uniform triangular cells, which results in a matrix with a rank the serial eigenvalue solver can handle. The error comparisons with other resolutions are presented in Fig. 3.1. The mesh with $0.00125m$ of longitudinal uniform intervals resulted in so many cells that the serial eigenvalue solver failed due to memory restrictions. Hence, the parallel version had to be employed benefiting from distributed memory architecture.

3.2 VALIDATION OF THE ITERATIVE ANALYSIS

The iterative method described in Chapter 2 must be validated first in several cases. Before including any sort of heating, a simple rectangular chamber without heat release, but impedance
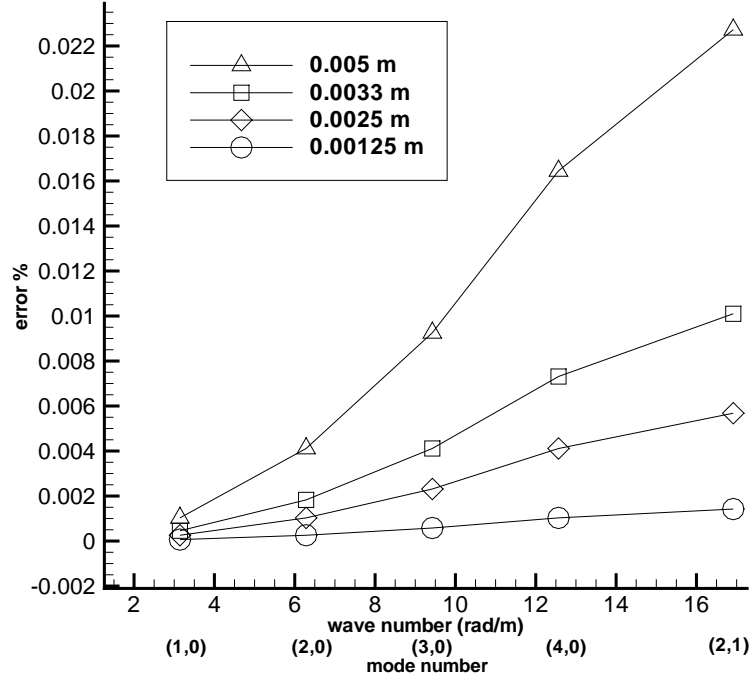
Figure 3.1: Natural mode wave number error percentages of meshes with uniform longitudinal intervals 0.00125 0.0025, 0.0033, and 0.005 m

boundary condition on walls shall be examined. The test setup can be viewed in Figure 3.2, where the wall on the right has an impedance boundary condition and hard wall condition on the rest. The iterative solution is expected to deviate the mode shape from normal mode with hard wall condition everywhere to the case mentioned.

To validate the solution, an analytical solution should be constructed first. The longitudinal waves can be determined through Helmholtz equation in 1-D

$$\frac{\partial^2 \hat{p}}{\partial x^2} + k^2 \hat{p} = 0$$

$$\text{with} \frac{\partial \hat{p}}{\partial x} = 0 \text{ at } x = 0$$

$$\text{and } \frac{\partial \hat{p}}{\partial x} - \frac{ik}{Z}\hat{p} = 0 \text{ at } x = L \tag{3.1}$$

The wave number can be found through a harmonic solution (see Appendix B)

$$k_n = n\frac{\pi}{L} + \frac{1}{L}\arctan(-i/Z), \qquad n \in N \tag{3.2}$$

Starting from the natural modes with hard wall conditions, the iterative procedure described in section 2.2 deviates the modes towards the conditions in the test setup. Taking $a = 0$, $b = -0.8$

27
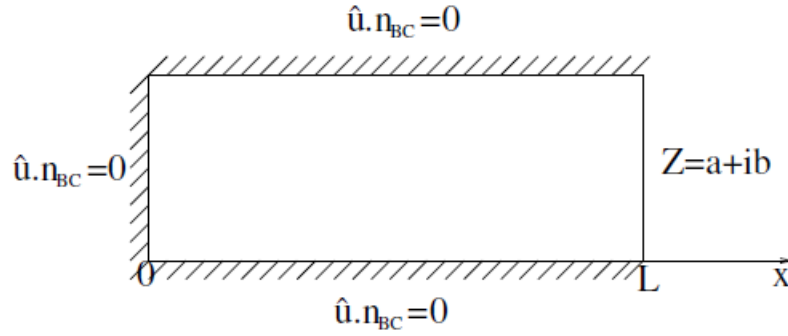
Figure 3.2: A chamber geometry without heat release, but with impedance wall condition.

in Figure 3.2, the solutions are found and compared with the analytical results in Table 3.1. Although the expected values are captured to some extent, we consider the computations are successful because together with the mixed modes, totally 10 modes were included in the analysis. Nevertheless, infinite number of modes should be included theoretically (see Eq. (2.21) and (2.22)). Higher resolution of the natural modes would make it possible to include more modes into the analysis, resulting in more accurate solutions. Thus, results with 20 modes of vibration are also included in the table. It should be mentioned that an unresolved mixed mode, occurring when 20 modes are extracted, is selected to be excluded from the analysis, not to ruin the whole solution. Still, (4,0) longitudinal mode solution was unable to converge, probably due to the inclusion of some unresolved higher modes. It can be observed that inclusion of more modes occasionally improves the solution. The expectation of better results does not hold for all modes, however. The reason for the exceptions is perhaps lack of crucial effects of some specific higher modes to some specific modes in consideration. Inclusion of infinite number of modes is not possible, after all. Besides, "small perturbations to the wavenumber" assumption should always be born in mind. Highly perturbing boundary conditions may supply inaccurate mode shapes.

A finer mesh (interval size 0.0025 m), including effects of 10 modes of vibration, can also be compared to the one with an uniform longitudinal interval size of 0.0033 m (Table 3.2). The tendencies do not obey to the expectations. Whereas natural modes are proved to be improved (see Fig. 3.1), the iterative solver working on the same mesh does not benefit from the increase of resolution. Likewise, the reason of this situation may be attributed to lack of effect of some crucial higher modes, or highly perturbing effect of the boundary condition.

28

Mod number	analytical(rad/m)	numerical (10 modes)	numerical (20 modes)
(1,0)	4.03764	3.97800	3.95604
(2,0)	7.17924	7.27429	7.22032
(3,0)	10.3208	10.5705	10.4633
(4,0)	13.4624	13.8985	not converged

Table 3.1: A test case with inactive flame and impedance wall condition $Z = -0.8i$ (The effect of 10 and 20 natural modes are included)

Mod number	analytical(rad/m)	numerical (0.0033 m)	numerical (0.0025 m)
(1,0)	4.03764	3.97800	3.97809
(2,0)	7.17924	7.27429	7.27530
(3,0)	10.3208	10.5705	10.5759
(4,0)	13.4624	13.8985	13.9375

Table 3.2: A test case with inactive flame and impedance wall condition $Z = -0.8i$ and two resolutions of solution

As discussed, the "small perturbation to the wavenumber" assumption may be violated. Apparently, due to the imposed boundary condition, any mode is modified considerably. For example, the first longitudinal mode deviated from 3.14159 to 3.97809 rad/m to comply with the condition. Therefore from Eq. 2.32, a large-in-magnitude impedance is expected to stick to the assumption more consistently. Results with $Z = 160i$ are presented in Table 3.3. Obviously, the error ratios are smaller for all modes. Additionally, there was a benefit from the inclusion of more mode numbers.

Mod number	analytical(rad/m)	numerical (10 modes)	numerical (20 modes)
(1,0)	3.1353428	3.1353206	3.1353195
(2,0)	6.2769356	6.2768245	6.2768219
(3,0)	9.4185283	9.4181530	9.4181486
(4,0)	12.560121	12.559224	12.559217

Table 3.3: A test case with inactive flame and impedance wall condition $Z = 160i$ (The effect of 10 and 20 natural modes are included)

No particular rule for the convergence behaviour of iterative method solution can be argued up to here. It is just expected by theory that inclusion of more and more natural modes would benefit to the solution success. 10 or 20 modes may not be significant against infinite

numbers, however it should give an estimate for the solution, as inclusion of infinite number of modes also would. Moreover, as it is emphasized before, "small perturbation to the wave number" assumption should always be born in mind as a first assessment for solution success. However, as there will always be considerable amount of perturbations to the wave number in real combusting cases with realistic boundary conditions, there is no need to be meticulous anyway . To conclude, all together what discussed in this chapter prove the foresight to be true, that the linear analysis constructed cannot be the most reliable way to find mode shape and wave number. Nevertheless, in the next chapter it shall be proved to be a tool to determine whether a mode of vibration in a duct will be excited or not.

CHAPTER 4

AN ELEMANTARY THERMOACOUSTIC DEVICE: THE RIJKE TUBE

Rijke tube has been simplest device to experiment, observe and analyse thermoacoustic oscillations and couplings. The first realization of thermoacoustic excitation of the tube was observed by P.L. Rijke in 19th century. He used a vertical tube open at both ends, with a wire mesh placed in the tube cross-section. Heating the wire resulted in an intense noise at one tone. The heated air through the wire rises up and cools down immediately by the wall, resulting in a mean flow upwards. At the same time, the increase of flux stemming from heating increases heat transfer. Under specific circumstances this phenomenon coincides pressure increase and causes excitation of the fundamental mode, resulting in emission of sound [40, 43, 44]. In this chapter, a horizontal type Rijke tube is to be analysed with respect to instability of the fundamental mode. The only distinction of the horizontal type of Rijke tube is that the lack of natural convection necessitates a trivial mean flow through the tube to initiate any acoustic motion (Figure 4.1). In the simulation, the geometry and mesh discussed in the previous chapter will be used.
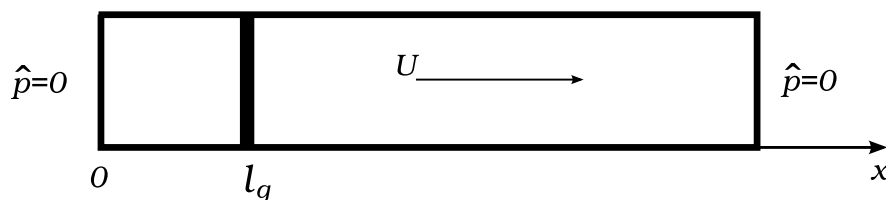

Figure 4.1: A horizontal Rijke tube

4.1   HEAT SOURCE

As discussed in Sec.2.4, the heat release is usually dependant on pressure and velocity. For a Rijke tube in Eq.(2.28), because of the dependency of heat transfer on velocity across the wire, the velocity term dominates over pressure term. Thus, it can be assumed that heat release depends purely on velocity in the case of Rijke tube. Moreover, as the wire mesh may be taken as a compact flame, Crocco's [4] $n - \tau$ model can be employed,

$$\dot{Q}'(t) = \int_{\Omega} q'(x,t)d\Omega = S_{ref}\frac{\gamma p_0}{\gamma - 1}n\mathbf{u}'(x_{ref}, t - \tau) \cdot \mathbf{n} \tag{4.1}$$

where S_{ref} is the flame area, x_{ref} is its location, and n is called interaction index, indicating the strength of coupling between acoustics and heat release. The equation can also be constructed in local form as [38]:

$$q'(x,t) = \frac{n}{\delta_f}\frac{\gamma p_0}{\gamma - 1}\mathbf{u}'(x, t - \tau) \cdot \mathbf{n} \tag{4.2}$$

where δ_f stands for the thickness of the flame. In numerical sense, this would be the thickness of the cell layer that takes over the release of heat for the entire system. With harmonic oscillation assumption and the momentum equation, the equation can be substituted in Eq.2.8 as

$$\hat{h} = \frac{n}{\delta_f}e^{ik\bar{a}\tau}\nabla\hat{p} \cdot \mathbf{n} \tag{4.3}$$

The gradient of pressure oscillation magnitude can be easily approximated numerically via Green-Gauss theorem. $+x$ direction is taken to be positive direction for the gradient calculation which means the mean flow is towards $+x$ direction.

4.2   BOUNDARY CONDITIONS

Hard wall boundary is chosen for the circumference of the tube (Fig.4.1). To simulate the open atmosphere conditions at both ends, the pressure oscillation magnitude will be forced to be zero. As discussed earlier in Sec. 2.5, a linear system of equation solver is implemented to solve for the $\hat{f}$ values for each cell on the boundaries. The system is simply constructed from Eq.(2.22),

$$\hat{p}(\mathbf{r}) = \psi_N(\mathbf{r}) + \sum_{n=0}^{\infty}{}' \frac{\psi_n(\mathbf{r})}{E_n^2(k^2 - k_n^2)}\left\{ \oiint_S \psi_n(\mathbf{r_{0_s}})\hat{f}(\mathbf{r_{0_s}})dS_0 \right\} \tag{4.4}$$

Clearly, at each iterative step, only unknowns are the $\hat{f}$ values throughout the boundary cells in question, accompanied by the same number of equations for the cells to close the system.

4.3 INSTABILITY ANALYSIS OF THE FUNDAMENTAL MODE

Through simplified analytical definitions and experiments, it has been observed that the first longitudinal mode of Rijke tube is excited under the following conditions [40, 43, 44]:

$$0 < 2k_1 l_g < \pi \tag{4.5a}$$

$$0 < \omega_1 \tau < \pi \tag{4.5b}$$

Here, the inequalities obtained [43] are adapted to the present harmonic assumptions. Normally, since $k_1 = \pi/L$, the inequalities would be interpreted as

$$0 < l_g < \frac{L}{2} \tag{4.6a}$$

$$0 < \tau < \frac{L}{\bar{a}} \tag{4.6b}$$

However, for the time being, let's use the calculated value of k_1 in (4.5) together with $\omega_1 = k_1 \bar{a}$.

The first condition implies that the mode is excited if the heater wire is located in the first half of the tube, when there is a mean flow in $+x$ direction. The second one determines whether the heat addition is in phase with the acoustic oscillations or not, according to the Rayleigh criterion [10, 40].

Using the $n - \tau$ heat model and the boundary condition implementation described in the previous sections, the simulation will be examined if it is consistent with these conditions. The first condition is examined first, taking $\tau = 10^{-4}\,s$ and $L = 1\,\mathrm{m}$ (Table 4.1). As stated earlier, the negative imaginary values of wave numbers implies the mode is stable, whereas positive-valued ones are excited modes. The results show that the condition is satisfied in all cases. That is, the excited mode is immediately attenuated when the heat source travels from the first half to the other half of the tube. Figure 4.2 is a better visualization of the behaviour. It is observed that the wave number does not fluctuate much with respect to the heater position. That is, the mode already vibrates in its frequency provided it is excited. The position of heat source only determines its activeness. In contrast, growth rate changes its sign as switched to the other half of the tube, meaning the mode will decay. It should also be noted that the fundamental natural mode (0,0), where wave number and pressure are spontaneously all zero, mutates and becomes the fundamental vibrant mode upon enforcing the open atmosphere boundary conditions at both ends. It is convention to call the vibrant mode with its corresponding hard-wall natural acoustic mode.

l_g (m)	0.25	0.4	0.75
Real part	3.4182	3.4178	3.4171
Imaginary part	8.72×10^{-5}	1.98×10^{-5}	-8.78×10^{-5}

Table 4.1: (0,0) mode wavenumber approximations for the Rijke tube with the heat source on various locations ($\tau = 10^{-4}$s).
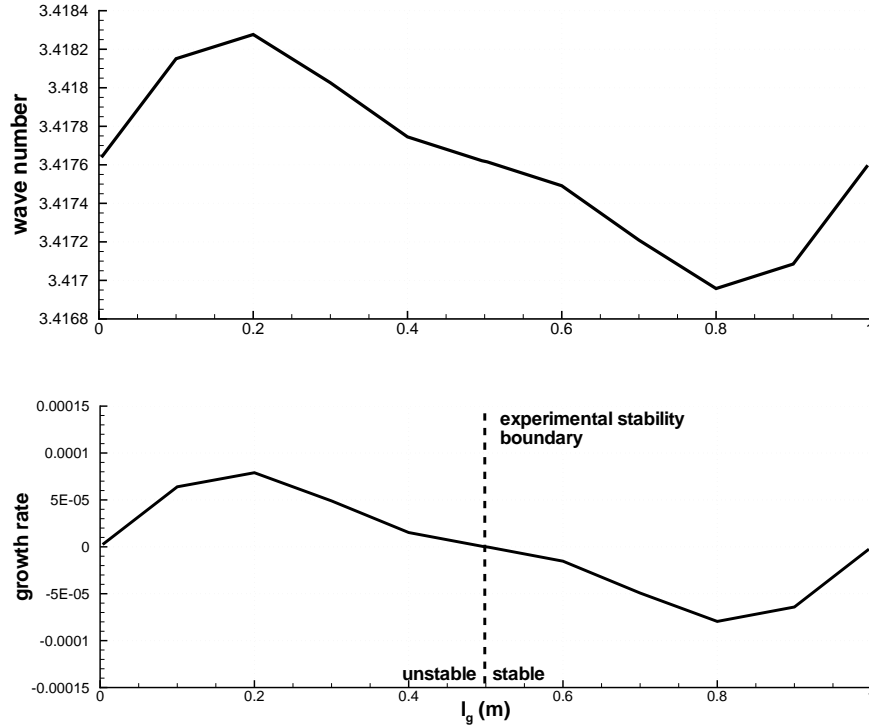
Figure 4.2: Wave number (upper) and growth rate (lower) variation of the fundamental mode when $\tau = 10^{-4}$ s

Likewise, the adherence to the first condition in Eq. (4.5)b can also be examined. According to the selected condition, that is $L = 1$ m and $\bar{a} = 350$ m/s, $0 < \tau < 2.62 \times 10^{-3}$s should be satisfied. Approximate wave numbers versus various time lag values are presented in Table 4.2. If the imaginary values, that is growth rates of the oscillations are to be inspected, it can be observed that the stability limit agrees with the analytically found limit (Fig. 4.3). In fact, some difference would be expected in-between, because even more assumptions are adopted in Culick's simple analysis, to obtain the tendencies easily [43]. Up to this point, the numerical analysis seems to be quite efficient and dexterous. However, wave number of the first mode, k_1, should have given $k_1 = \pi/L$ reasonably, as adopted in (4.6). Therefore, the instability condition would be $0 < \tau < 2.86 \times 10^{-3}$ instead. It can be concluded that the

obtained wave number result does not reflect the reality accurately.

τ (s)	10^{-5}	10^{-4}	10^{-3}	2.6×10^{-3}	2.7×10^{-3}
Real part	3.4182	3.4182	3.4178	3.4171	3.4171
Imaginary part	6.75×10^{-6}	6.72×10^{-5}	5.26×10^{-4}	1.82×10^{-5}	-4.96×10^{-5}

Table 4.2: (0,0) mode wavenumber approximations for the Rijke tube with various time-lag values ($l_g = 0.25\,m$)
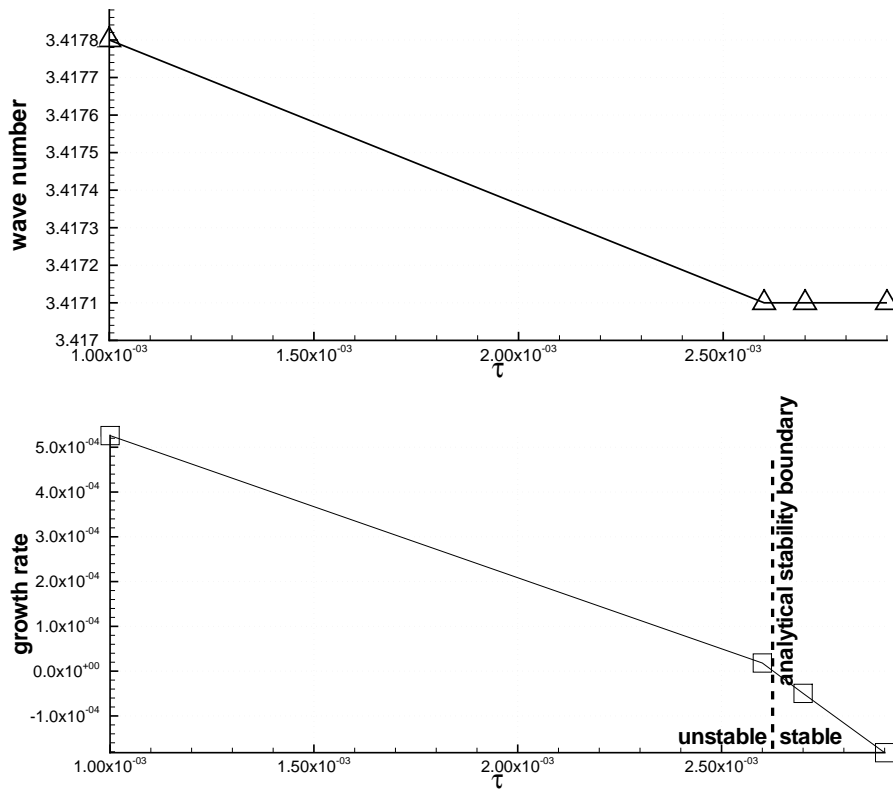
Figure 4.3: Wave number (upper) and growth rate (lower) variation of the fundamental mode when $l_g = 0.25\,m$

To exemplify, the excited mode shape can be viewed in Fig. 4.4. Together with the chosen mean sound speed, 350 m/s, the obtained k value corresponds to a medium-pitch sound with a frequency of 190 Hz in audible range. Of course, it is for sure that the wave number has a considerable amount of error, as discussed in Chapter 3. In fact, the wave shape is obviously a full wave (see Fig.4.4) with a wave-length of $\lambda = L = 1$ m. Hence, the real wave number and the frequency are expected to be $k = \pi$ rad/m, and 175 Hz respectively (with inactive flame and $\hat{p} = 0$ boundary conditions, analytically $\hat{p} = A\sin(n\pi x)$). After all, it was apparent that

because of violently deviating behaviour of the open-atmosphere boundary conditions, the natural mode shape (0,0) deviates tremendously, expectedly resulting in a dramatic amount of error. As to the instability analysis however, there seem to be no significant error. Provided the heat model and selected boundary conditions are good enough to simulate the phenomenon, any other inspections can be performed safely unless there is a serious violation of stated assumptions.
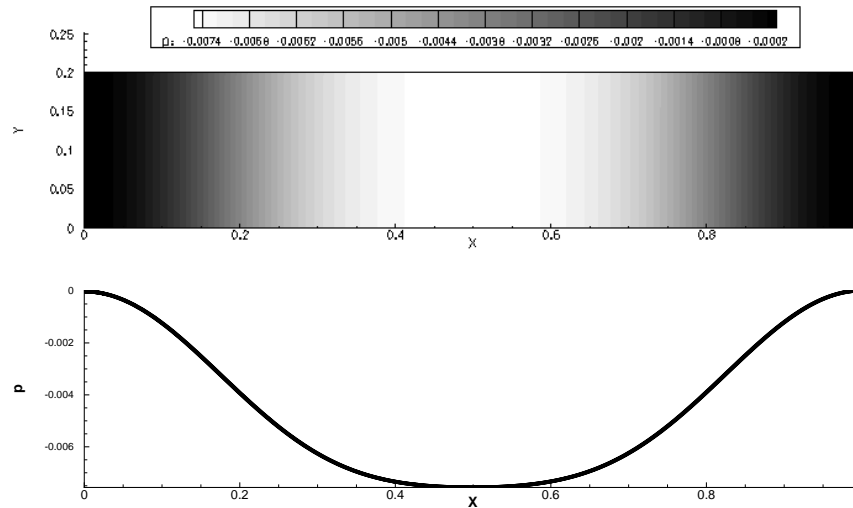
Figure 4.4: The excited mode (0,0) when $l_g = 0.25$ m and $\tau = 10^{-4}$ s

CHAPTER 5

A SAMPLE INSTABILITY ANALYSIS OF A LIQUID-PROPELLED COMBUSTION CHAMBER MODEL

The last step of analysis will certainly be of a sample liquid-propelled combustion chamber. In a real liquid-propelled rocket engine, high levels of pressure and temperature exist in the chamber, followed by a narrow throat of the nozzle entry. Pressure levels are usually on the order of 10 bars and volumetric heat release on the order of 300 megawatts per meter cube (e.g. Aestus rocket engine [45, 46]). Thus, flow is essentially supersonic in the nozzle, necessitating sonic condition on the throat. The simulation setup should be constructed considering this condition. Hence, this chapter examines a chamber with choked flow at the throat. Mean flow effects are neglected as before, despite its significance in liquid rocket chambers.

5.1 THE ROCKET ENGINE SETUP AND NATURAL MODE SHAPES

A fictional rocket motor geometry is generated with dimensions given in Fig. 5.1. To realize choked condition, the geometry and mesh of subsonic nozzle is split through throat. That makes a domain of 21245 triangular cells. Because higher gradients are expected, the mesh in the proximity of the throat section is set to be finer (Fig. 5.2). Despite not very physical, the mass input of the propellants and resultant velocity inlet condition is neglected in the analysis. A constant velocity perturbation condition $\hat{f} = -ik\bar{a}\hat{\mathbf{u}} \cdot \mathbf{n}$ could also have been imposed on the inlet - which is already taken as zero by definition. Taking the inlet as hard wall is adequate for the time being for the fictional engine.

Before inclusion of any effects of the natural modes iteratively, they should be verified and identified first. The shapes of 12 modes of vibration are demonstrated in Fig. 5.3 followed
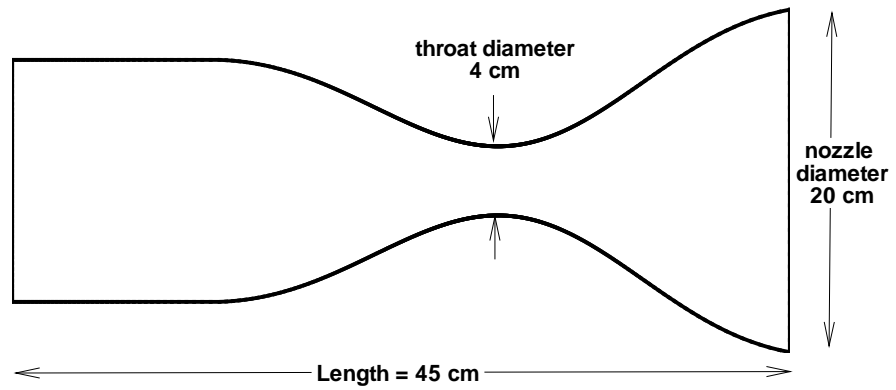
Figure 5.1: A fictional liquid-propelled rocket motor

by corresponding wave numbers in Table 5.1. Each mode shape is identified via capitals and consecutive numbers: "L" meaning longitudinal; "R" radial, both followed by mode numbers. For instance, L1R1 stands for first longitudinal first radial mixed mode.

index number	Mode identity	Wave number k (rad/m)
1	L1	12.93510
2	L2	23.05547
3	R1	23.53690
4	L1R1	30.83868
5	L3	34.00244
6	L3R1	41.37291
7	L4	44.84321
8	R2	45.99022
9	L4R1	51.52343
10	L2R2	51.57302
11	L5	56.01193
12	L3R2	60.75879

Table 5.1: Wave numbers of the natural modes considered
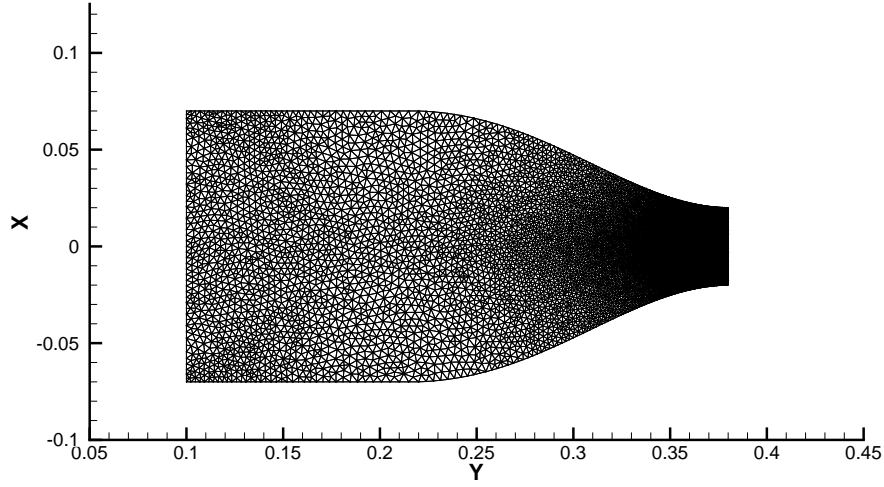
Figure 5.2: The choked rocket motor

5.2 HEAT SOURCE

A simple $n - \tau$ model for heat release by Crocco and Cheng is adopted [4]

$$\dot{q_v}' = \bar{q}_V \frac{n}{p_{\bar{C}H}} \left[p'(t) - p'(t - \tau) \right] \tag{5.1}$$

where $\bar{q_V}$ is the volumetric heat release, $p_{\bar{C}H}$ is the chamber mean pressure and n is the interaction index and τ the time lag between acoustics and heat release. Unlike in the case of Rijke tube studied in Chapter 4, pressure is assumed to be dependent purely on pressure fluctuation. Harmonic variation assumption leads to the source term for the inhomogeneous Helmholtz equation (Eq. (2.8a)),

$$\hat{h} = \frac{\gamma - 1}{\bar{a}} (ik) \frac{n\bar{q}_V}{p_{\bar{C}H}} \hat{p} (1 - e^{ik\bar{a}\tau}) \tag{5.2}$$

Upon the application of Rayleigh integral locally [45], it is proved that this flame model never has damping effect. However, as the chamber has damping type of boundary condition, that is, some acoustic loss must exist, stability of modes is also expected.

A cloud of heat source is formed by marking triangular cells all together forming an approximate cylinder shape with a height of 0.4 cm., about a center disc located close to the motor

39
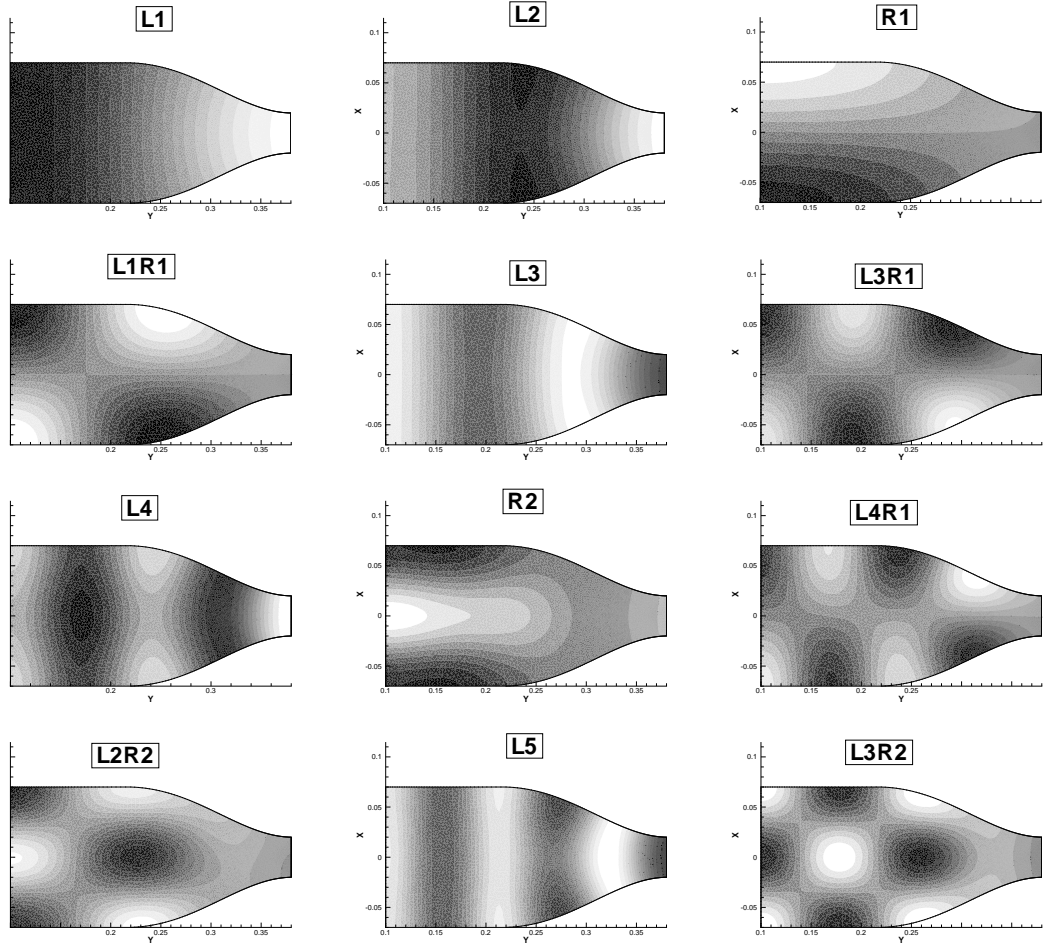
Figure 5.3: The mode shapes included in the stability analysis

head. Totally, the set consists of 1246 cells all contributing to the system as a separate volume of heat source in equal magnitude.

5.3 BOUNDARY CONDITIONS

The reasoning behind cutting off the nozzle through the throat in choked flow condition is that a sonic line attaches to the throat, preventing the acoustic waves from propagating upstream of the throat. Hence, there is no acoustic reflection at all on that plane, which can also be interpreted as a total loss of acoustic waves through the plane. The realization of this condition normally requires determination of impedance value for each frequency. Solution of quasi-one dimensional Euler equation on sonic line gives [34]

$$Z_* = \frac{2\frac{d\bar{u}}{dx}\big|_* - i\omega}{(\gamma - 1)\frac{d\bar{u}}{dx}\big|_* - i\omega} \tag{5.3}$$

where the starred values refer to the ones on sonic line. The solution procedure assumes uniform mean flow, then the impedance simply becomes

$$Z_* = 1 \tag{5.4}$$

This is indeed the widely used value for the particular case of infinitely long duct where no reflection occurs without dependence on frequency. This will be used in the analysis for convenience.

5.4 RESULTS

For the fictional engine, following representative properties are used in the analysis:

Mean speed of sound:	$\bar{a} = 440$ m/s
Mean chamber pressure:	$p_{CH} = 800$ KPa
Mean volumetric heat release:	$\bar{q}_V = 200\,MW/m^3$

A range of interaction index and time lag values will be used to form a stability map of the engine. n and τ generally depend on spatial coordinates. Besides, fields of these parameters are usually quite difficult to obtain experimentally. It is also possible to obtain them by the help of compressible reacting LES for a similar case to deduce the response of turbulent flame to acoustic perturbations [49, 50]. In this work, they shall be taken constant like the other flame parameters. For the case of hypergolic propellants and coaxial injectors, empirical values obtained by Harrje and Reardon [5] are generally in the ranges of

$$0.14 \times 10^{-3}\,s \leq \tau \leq 0.20 \times 10^{-3}\,s \tag{5.5}$$

$$0.6 \leq n \leq 0.8 \tag{5.6}$$

Therefore, the ranges should used initially to form stability maps. Any other desired range during design stage can also be examined. In Fig. 5.6 stability maps of the engine for the first 6 acoustic modes are depicted. The plots imply that the longitudinal modes tend to be

stable, because the nozzle has an intensive damping effect on the longitudinal modes due to flow choking. The supersonic conditions beyond the choked throat section attenuate most of the acoustic energy of longitudinal oscillations, resulting in stability. This is in fact the case for the first four longitudinal modes. More generally, all of the pure longitudinal modes are subject to the same intensive stabilizing effect. As to the first radial mode, stability is observed in all cases, except there are some points where the iterations did not converge. L1R1 mixed mode, however, seems to be excited in the ranges probed. The most remarkable of the modes observed is L3R1 mixed mode. In some interval of time lag value, it appears to be unstable. On the contrary, as the strength of coupling is reduced, that interval diminishes, rendering the mode stable beyond. If a mode vibrates possibly in a limit cycle, characteristics of which cannot be deduced in this very linear analysis, it may cause huge troubles during firing tests unless cured in simulation phase. The design should then be tuned involving a geometry change or inclusion of means of acoustic damping for that specific frequency and shape such as liners on the walls, or baffles on the injectors.

The excited mode L1R1 can be illustrated in Fig. 5.4. As observed, there is no obvious difference in the shape compared with the hard-wall natural correspondent (Fig. 5.5). There is only small deviations due to the heat addition and the imposed boundary condition on the throat. The shape should solely be taken as an approximation to the initial shape just at the moment of triggering of the mode. As discussed, non-linear effects and unsteadiness would govern beyond that level converging into a limit cycle. Such behaviour is another subject of study involving temporal evolution of flow field.

Eventually, It should be mentioned that in a rocket engine, tangential modes, or mixtures of tangential modes are typically not only more easily self-excited ones, but also they are the most troublesome modes in prevention and controlling aspects. Therefore, a comprehensive 3-D analysis is of the most value than any means of 2-D modelling of the phenomenon. Moreover, it should also be noted that the iterative nature of the method allows implementation of more complex non-linear flame models and application of non-linear boundary conditions when needed.
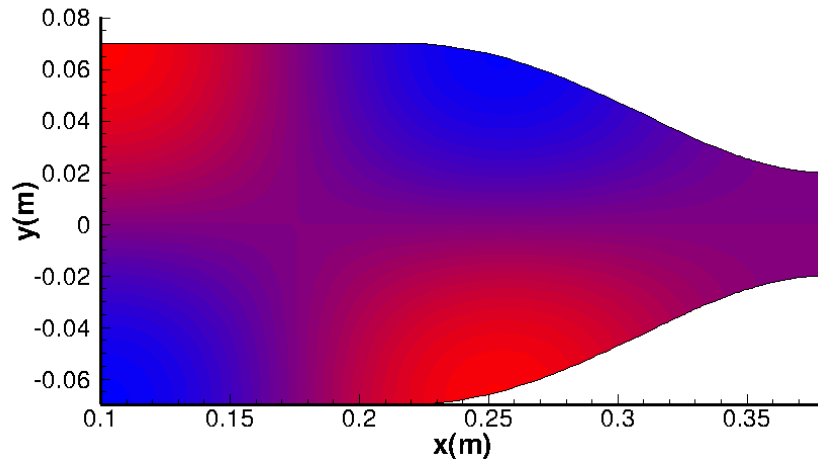
Figure 5.4: Perturbed mode shape of the active mode L1R1 ($n = 0.8$ and $\tau = 0.18$ ms) vibrating with $k = 30.8461$ rad/s
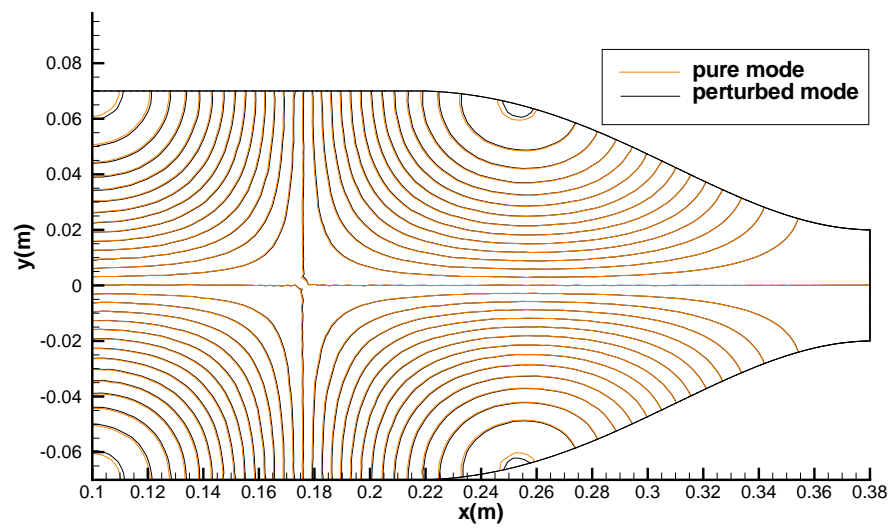
Figure 5.5: Perturbed mode shape of the active mode L1R1 vs. its pure mode

43
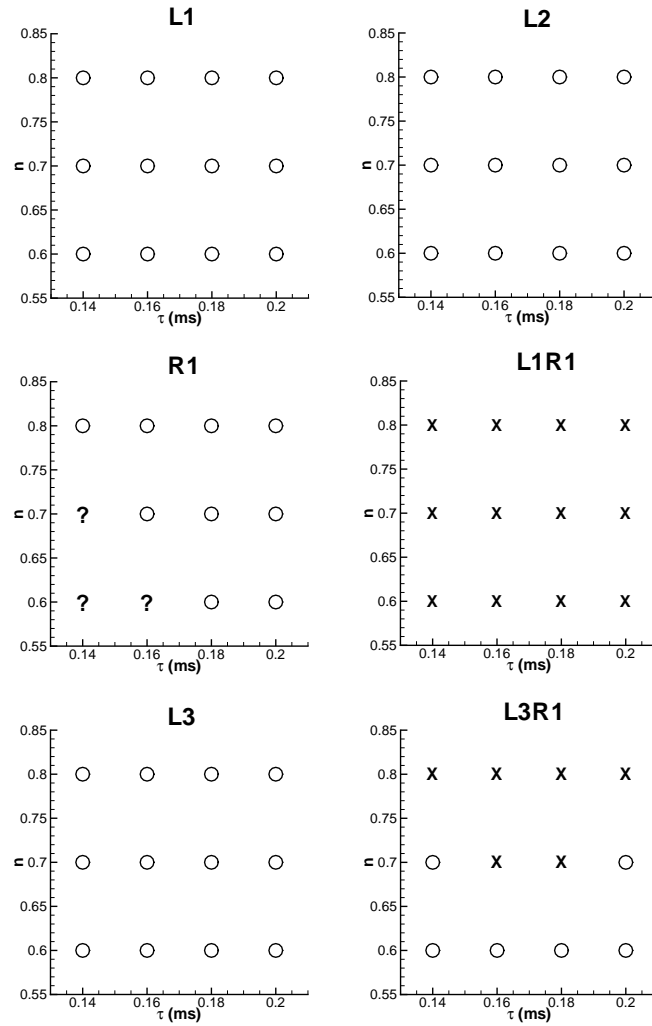
Figure 5.6: The choked rocket motor stability map for several modes. "o" stands for stable; "x" unstable mode.

5.5 THE CHOKED ROCKET MOTOR CASE IN 3-D

For demonstrative purposes, the exactly same setup can also be examined in 3-D. What 3-D case involves are extra computational burden, tetrahedron cells instead of triangles, and volumes instead of areas. Additionally, tangential modes, which do not even exist in 2-D case, can also be inspected as to stability conditionings. The 3-D mesh with 91815 tetrahedral cells is shown in Fig.5.7. The hard wall natural modes are computed efficiently via PARPACK, as discussed in chapter 2. Totally 15 modes are computed for use in the analysis. Table 5.2 presents the mode numbers computed for the iterative instability analysis. Some of the mode shapes can be viewed in Fig. 5.8. It is interesting that tangential modes and mixed tangential

44

modes appeared as pairs. The equivalent pairs are excluded in the figure.

index number	Mode identity	Wave number k (rad/m)
1	L1	15.2831
2	L2	25.3825
3	T1	28.5526
4	T1	28.5711
5	L3	36.1271
6	L1T1	35.6129
7	L1T1	35.6312
8	L4	47.0956
9	T2	46.7427
10	T2	46.7017
11	L2T1	46.5996
12	L2T1	46.5809

Table 5.2: Wave numbers of the natural modes considered for the 3-D chamber

An iterative analysis for instability is performed for the identical parameters of combustion on this 3-D version of the chamber in the previous section. However, the results should not be reliable due to the fact that the 3-D natural mode solutions have considerable amount of inaccuracy, as proved and discussed in Chapter 2. Still, the stability map of the rocket engine can be seen in Figure 5.9. "?" denotes the cases for which iterations did not converge. Longitudinal modes turned out to be stable in the intervals, as expected and found in the 2-D case. Tangential modes (i.e.. T1) were expected to be unstable because there is no obvious internal or external damping in transverse directions. They are found to be unstable, at least in the present time lag and interaction index intervals. However, as discussed in Section 5.2, the flame model never has damping effect, therefore the tangential modes are not expected to be unstable in any interval. On the contrary, mixed modes are subject to the nozzle's damping effect. The mixed mode L1T1 had serious converging problems however, most probably due to the fact that the natural modes were not accurate enough. It was expected to be stable in some intervals.

In summary, the 3-D hard-wall natural mode shape has to be validated before any use of the 3-D stability analysis, despite the fact that the longitudinal modes and tangential mode analysis complied with the expectations. For the time being, only 2-D analysis can be used in a work concerning combustion stability in a duct, where the oscillating modes are to be
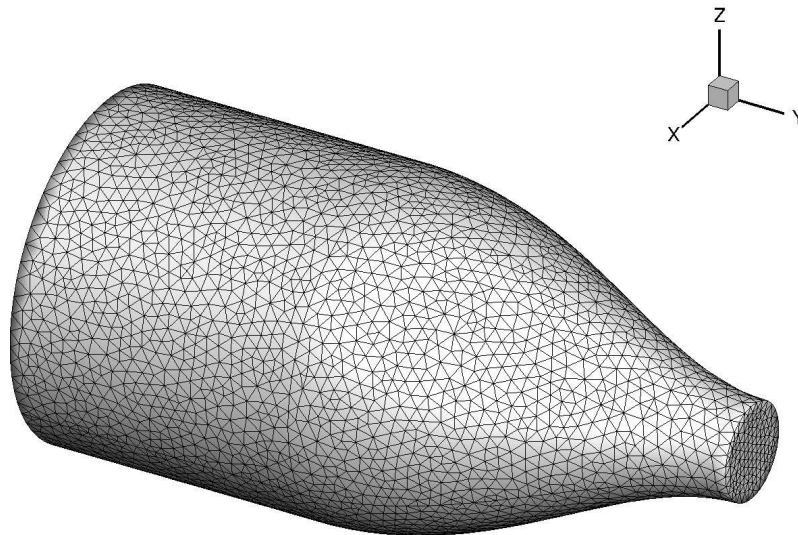
Figure 5.7: 3-D rocket geometry and mesh for choked flow
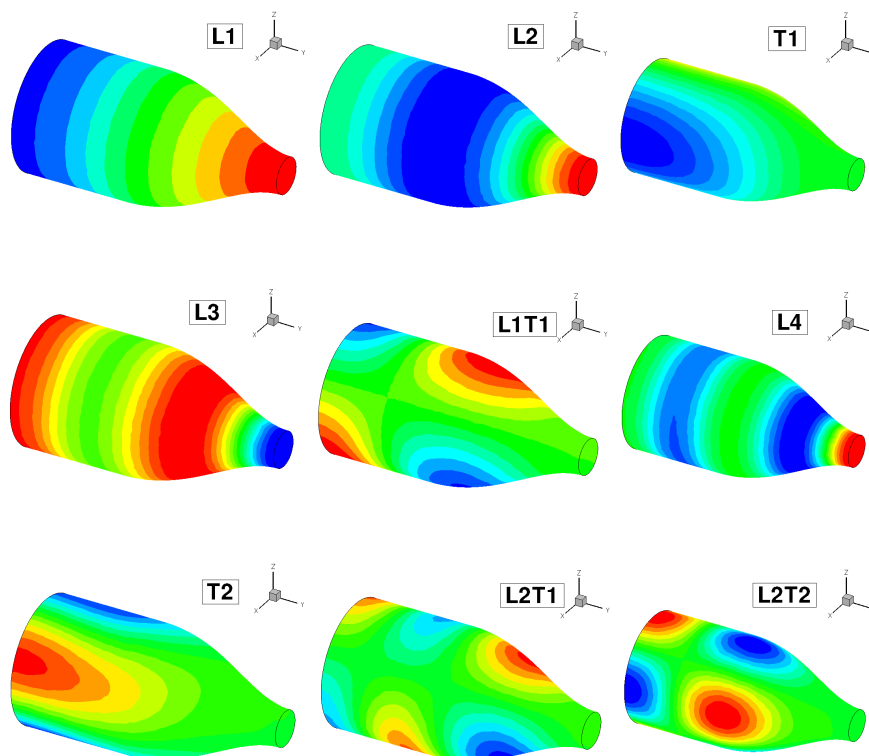
Figure 5.8: Some of the modes included in the analysis of choked 3-D rocket
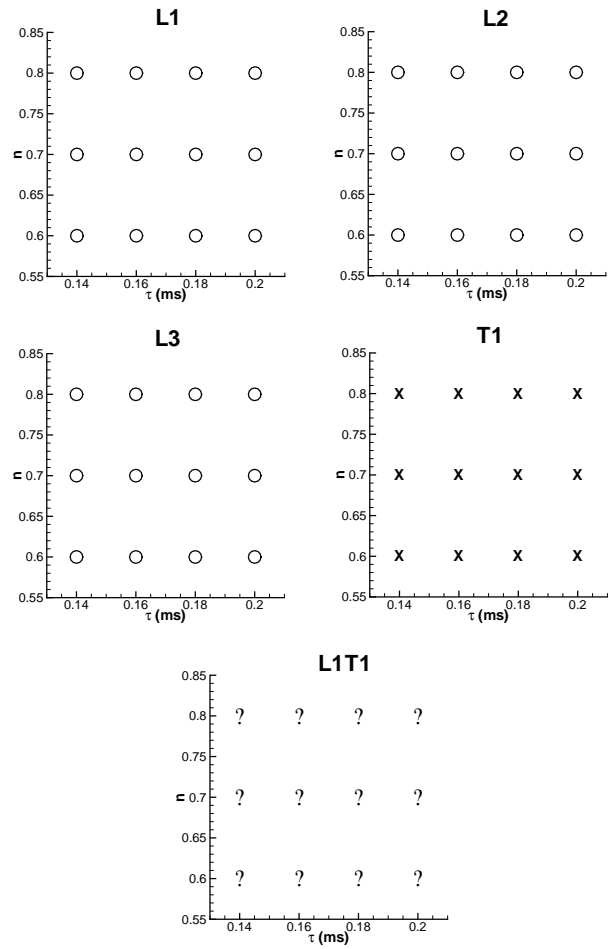
Figure 5.9: The 3-D choked rocket motor stability map for several modes. "o" stands for stable; "x" unstable mode.

thrown outside operation interval of the duct by decisive changes in the design of the duct.

CHAPTER 6

CONCLUSION

In this thesis, for the analysis of linear combustion instabilities particularly in liquid-propellant rocket engines, a methodology, involving Culick's iterative method, is constructed. It was designed as a first step towards simulation and design of combustion instabilities in 3-D ducts, mostly applicable to liquid rocket motor chambers. It is proved that the neglection of non-linear effects and mean flow effects simplifies the analysis down to practical levels where self-excitement behaviour of possible modes are detected in the first place. Obtained mode shapes are not supposed to be reliable solutions as to accuracy because of various assumptions made. Nevertheless, the information obtained whether the mode in question will sustain its oscillations or be diminished, serves well as a primary idea throughout conceptual design of a chamber geometry. In case of the instability of a mode, the growth and convergence behaviour of oscillations will always be a mystery in the lack of non-linear effects, for limit cycles are known to be a mere non-linear phenomenon. On the contrary, lack of non-linear effects does not disrupt any design intended for stability, because inclusion of them would serve as extra dissipation, having the tendency to add to the stability of the system. Those effects might be included in further studies in a step by step manner.

To serve for these purposes, a finite volume natural mode shape extractor (*HELM2D*) and a iterative solver (*YAKAR*) are developed, taking into account the heating effects and boundary condition forcing. Both of them have 2-D and 3-D versions. However, the 3-D natural mode shape extractor requires further improvements with higher orders of accuracy, due to the fact that the modes are not captured well enough with a second order of accuracy finite volume discretization. A finite element discretization with quadratic interpolation functions is expected to suffice for that purpose. Therefore, 2-D analysis of two cases are emphasized for now. Still, an example of rocket combustion is simulated in 3-D. In chapter 3, solution for

a duct with inactive flame but with impedance wall condition is validated, whereas in chapter 4, the famous Rijke tube is analysed as to the behaviour of the first tone of vibration. The method performed well in both cases with some exceptional behaviours. A sample instability analysis of a simple liquid-propellant combustion chamber is also assessed in Chapter 5. Some mixed modes tended to be unstable whereas all of the low frequency longitudinal mode oscillations were decayed because of intensive damping effect of nozzle. A 3-D analysis was found to be vital, which additionally includes the results of tangential modes. Hence, the rocket is also tested in 3-D analysis for the sake of comparison and those tangential modes. It was already predicted that the 3-D solution would be problematic because of the inaccuracy of natural mode shape basis. Eventually, some mixed mode cases failed to converge for the 3-D case, whereas the rest was found to comply with the 2-D results.

To conclude, the methodology discussed proved to be successful in practical applications where a duct with proper heat and boundary models is to be assessed whether it sustains any acoustic vibrations or not before any following design steps. Due to the assumptions involved, the reliance on mode shape solutions should be avoided for now, though. The time required for solution of cases is also extremely small compared to the other works which might even extend to several days. Moreover, the fact, that heat and boundary condition implementations are simple flexible functions dependent on current flow variables on the iterative step, overwhelms some other methods involving quadratic non-linear eigenvalue problems with large matrices which have always been quite difficult to solve. The flexibility of the method might also make it easier to include non-linear models of combustion and application of boundary conditions as non-linear functions, not less than further implementations and models in further progresses.

REFERENCES

[1] Travis S. Taylor, *"Introduction to Rocket Science and Engineering"*, CRC Press, 2009, ISBN 978-1-4200-7528-1

[2] Wikipedia article, *"Space Shuttle main engine"*, http://en.wikipedia.org/wiki/Space_-Shuttle_main_engine, as accurate of December 2010

[3] L. Rayleigh, *"The Theory of Sound, Volume Two"*, Dover Publications, New York, 1877 re-issued 1945

[4] Crocco, L., and Cheng, S. I., *"Theory of Combustion Instability in Liquid Propellant Rocket Motors*, AGARD monograph, No.8, Butterworths, London, 1956

[5] Harrje, D., and Reardon, F., *"Liquid Rocket Combustion Instabilities"*, NASA SP-194, 1972

[6] Culick, F.E.C., *"Combustion Instabilities in Liquid-Fueled Propulsion Systems: an Overview"*, AGARD CP 450, 1988

[7] Fred E. C. Culick, Vigor Yang, *"Overview of Combustion Instabilities in Liquid-Propellant Rocket Engines"*, California Institute of Technology and Pennsylvania State University, from the compilation *"Liquid Rocket Engine Combustion Instability"* edited by Vigor Yang, W. E. Anderson, Progress in Astronautics and Aeronautics Vol.169, American Institute of Aeronautics and Astronautics, 1995

[8] Vigor Yang, Josef M. Wicker, and Myong Won Yoon *"Acoustic Waves in Combustion Chambers"*, Pennsylvania State University, from the compilation *"Liquid Rocket Engine Combustion Instability"* edited by Vigor Yang, W. E. Anderson, Progress in Astronautics and Aeronautics Vol.169, American Institute of Aeronautics and Astronautics, 1995

[9] *"Unsteady Motions in Combustion Chambers for Propulsion Systems"*, AG-AVT-039, NATO Research and Technology Organization, December 2006

[10] Dr. R. I. Sujith, *"Acoustic Instabilities in Aerospace Propulsion"*, Department of Aerospace Engineering, Indian Institute of Technology Madras

[11] S.W. Rienstra, A. Hirschberg, *"An Introduction to Acoustics"*, Eindhoven University of Technology, March 2010

[12] R. B. Lehoucq, D. C. Sorensen and C. Yang. *"ARPACK USER'S GUIDE: Solution of Large Scale Eigenvalue Problems with Implicitly Restarted Arnoldi Methods"* SIAM, Phildelphia, PA, 1998.

[13] R. B. Lehoucq, J. A. Scott, *"Implicitly restarted Arnoldi methods and eigenvalues of the discretized Navier Stokes equations"*, Technical Report SAND97-2712J, Sandia National Laboratories, Albuquerque, New Mexico, 1997.

[14] R. B. Lehoucq and A. G. Salinger, *"Massively parallel linear stability analysis with PARPACK for 3D fluid flow modelled with MPSalsa"*, Sandia National Laboratories

[15] K. J. Maschhoff and D. C. Sorensen, *"P_ARPACK: An Efficient Portable Large Scale Eigenvalue Package for Distributed Memory Parallel Architectures"*, Rice University, 2007

[16] M. Snir, S. Otto, S. Huss-Lederman, D.Walker and J. Dongarra, *"MPI-The Complete Reference"*, Vol.I:The MPI Core, MIT Press, Massachusetts and London, 1998

[17] ARPACK website *"http://www.caam.rice.edu/software/ARPACK/"*, as accurate of March 2010.

[18] LAPACK website *"http://www.netlib.org/lapack/"*, as accurate of October 2010.

[19] Gudmundsson K., Colonius T., *"Linear Stability Analysis of Chevron Jet Profiles"*, ASME FEDSM2006-98485, July 2006

[20] Culick, F. E. C., *"Stability of pressure oscillations in gas and liquid rocket combustion chambers,"*, Mass. Inst. Tech., Aerophys. Lab., TR 480 (June 1961).

[21] Culick, F. E. C., *"High Frequency Oscilllations in Liquid Rockets"*, AIAA Journal, Vol. 1, No.5, 1963, pp. 1097-1104

[22] G.A. Flandro, *"Vortex Driving Mechanism in Oscillatory Rocket Flows"*, AIAA Journal of Propulsion and Power, vol.2, no.3, May-June, 1986

[23] G.A. Flandro, *"Effects of Vorticity on Rocket Combustion Stability"*, AIAA Journal of Propulsion and Power, vol.11, no.4, July-August, 1995

[24] French, J.C., *"Three Dimensional Combustion Stability Modeling for Solid Rocket Motors"*, 34th AIAA / ASME / SAE / ASEE Joint Propulsion Conference and Exhibit, Cleveland, OH, AIAA 1998-3702..

[25] J.E. Caruthers, J.C. French, and G.K. Raviprakash, *"Green Function Discretization for Numerical Solution of the Helmholtz Equation"*, Journal of Sound and Vibration, 187(4), 553-568, 1995.

[26] French, J.C. and Dang, A.L., *"Analytic Combustion Stability Analysis of a Non-axisymmetric Motor Cavity, Including Non-axial Acoustic Modes: A Status Report"*, 35th JANNAF Combustion Subcommittee, Tucson, AZ, 1998.

[27] French, J.C. and Coats, D.E., *"Automated 3-D Solid Rocket Combustion Stability Analysis"*, Software and Engineering Associates, Carson City, 35th AIAA / ASME / SAE / ASEE Joint Propulsion Conference and Exhibit, Los Angeles, CA, AIAA 1999-2797.

[28] French, J.C., Flandro, G.A., Majdalani, J., *"Improvements to the Linear Standard Stability Prediction Program (SSP)"*, 40th AIAA / ASME / SAE / ASEE Joint Propulsion Conference, AIAA-2004-4181, Fort Lauderdale, FL, July 2004.

[29] French, J.C., Flandro, G.A., *"Mode Shape Distortion in Extended Area T-Burners"*, 36th JANNAF Combustion Subcommittee, Cocoa Beach, FL, 1999.

[30] French, J.C., *"Analytic Evaluation of a Tangential Mode Instability in a Solid Rocket Motor"*, 36th AIAA / ASME / SAE / ASEE Joint Propulsion Conference and Exhibit, Huntsville, AL, AIAA 2000-3698.

[31] Rubin, S., *"Longitudinal Instability of Liquid Rockets Due to Propulsion Feedback(POGO)"*, J. Spacecraft Rockets, vol.3, no.8, Aug. 1966, pp. 1188-1 195

[32] L. Benoit., *"Prédictions des instabilités thermoacoustiques dans les turbines à gaz"* - TH/CFD/05/41. PhD thesis, Université de Montpellier II, Montpellier, France - Information, Structures, Systémes, 2005.

[33] C.E. Martin, L. Benoit, Y. Sommerer, F. Nicoud, T. Poinsot *"Large-Eddy Simulation and Acoustic Analysis of a Swirled Staged Turbulent Combustor"*, AIAA Journal, vol.44, no.44, April 2006

[34] N. Lamarque, T. Poinsot, *"Boundary conditions for acoustic eigenmode computations in a gas turbine combustion chambers"*, AIAA Journal, 46 (9), pp. 2282-2292, 2008.

[35] L. Benoit, F. Nicoud, *"Numerical Assessment of Thermoacoustic Instabilities in Gas Turbines"*, International Journal for Numerical Methods in Fluids, Vol. 47, Nos. 8-9, 2005, pp. 849-855

[36] Jan-Willem van Leeuwen, *"Computation of thermo-acoustic modes in combustors"*, Master's Thesis for Applied Mathematics, Delft, June 5th, 2007

[37] A. Kaufmann, F. Nicoud, *"Flow Forcing Techniques for Numerical Simulation of Combustion Instabilities"*, Combustion and Flame, vol. 131, 2002, pp. 371-385

[38] F. Nicoud, L. Benoit, C. Sensiau and T. Poinsot, *"Acoustic modes in combustors with complex impedance and multidimensional active flames"*, AIAA J. 45, 426 (2007)

[39] C. Hantschk, D. Vortmeyer, *"Numerical Simulation of Self-excited Thermoacoustic Instabilities in a Rijke Tube"*, Journal of Sound and Vibration, 1999, vol. 277(3), pp. 511-522

[40] K.Vijayakrishnan and N Ananthkrishnan,*"Understanding Thermoacoustic Instabilities in Rocket Engines: The Rijke Tube as a prototypical Example"*, Seminar on Advances in Propulsion, Indian Institute of Technology-Bombay, 2003

[41] Maria A. Heckl, M.S. Howe,*"Stability Analysis of the Rijke Tube with a Green's Function Approach"*, Journal of Sound and Vibration, vol.305, 2007, 672-688

[42] Maria A. Heckl, *"The Rijke Tube: Green's Function Approach in the Frequency Domain"*, Acta Acustica, vol. 96, 2010, pp. 743-752

[43] F. E. C. Culick, *"Dynamics of Combustion Systems: Fundamentals, Acoustics, and Control"*, California Institute of Technology

[44] K. Matveev., *"Thermoacoustic Instabilities in the Rijke Tube: Experiments and Modeling"*. PhD thesis, California Institute of Technology, Pasadena, CA, 2003.

[45] J. Perringer and T. Sattelmayer, *"Simulation of Combustion Instabilities in Liquid Rocket Engines with Acoustic Perturbation Equations"*, Journal of Propulsion and Power, Vol.25, No.5, 2009

[46] Aestus Rocket Engine *"http://cs.astrium.eads.net/sp/LauncherPropulsion/Aestus-Rocket-Engine.html"*, as accurate of September 5th, 2010.

[47] S.M. Camporeale, B. Fortunato, and M. Mastrovito, *"Prediction of Thermoacoustic Instability in Combustion Chamber Equipped with Passive Dampers"*, Proceedings of ASME Turbo Expo 2008: Power for Land, Sea and Air, GT2008-51387, Berlin, June 9-13

[48] Dong Jin Cha, Jay H. Kim and Yong Jin Joo, *"Analysis of the Combustion Instability of a Model Gas Turbine Combustor by the Transfer Matrix Method"*, Journal of Mechanical Science and Technology, vol.23 (2009), pp. 1602-1612

[49] Truffin, K., Varoquié, B., and Poinsot, T., *"Measurements of Transfer Functions in Reacting Flows Using Large Eddy Simulations,"* 10th International Congress on Sound and Vibration, P-38, 2003, pp. 785-793.

[50] Polifke, W., Poncet, A., Paschereit, C., and Doebbeling, K., *"Reconstruction of Acoustic Transfer Matrices by Instationary Computational Fluid Dynamics,"* Journal of Sound and Vibration, Vol. 245, No. 3, 2001, pp.483-510.

[51] Chae Hoon Sohn, I-Sun Park, Seong-Ku Kim and Hong Jip Kim, *Acoustic Tuning of Gas-liquid Scheme Injectors for Acoustic Damping in a Combustion Chamber of A Liquid Rocket Engine*, Journal of Sound and Vibration, vol.304 (2007), pp.793-810

[52] C. Bogey, C. Bailly, and D. Juve, *"Computation of Flow Noise Using Source Terms in Linearized Euler's Equations"*, AIAA Journal, vol.40,no.2, February 2002

Appendix A

DERIVATION OF LINEARIZED EULER EQUATIONS

Throughout the linearization of Euler equations, the following assumptions are adopted for the problem in consideration:

- Inviscid and adiabatic flow

- C_p, C_v and γ are constant

- Fluctuations of u, p, T, ρ and Q are small

- Uniform steady state pressure and density: p_0, ρ_0 are constant

A.1   Continuity equation

The conservation of mass in differential form without a source nor sink can be written as,

$$\frac{\partial \rho}{\partial t} + \nabla \cdot (\rho \vec{V}) = 0 \tag{A.1}$$

Linearization of the parameters around mean values leads to,

$$\frac{\partial (\rho_0 + \rho')}{\partial t} + \nabla \cdot ((\rho_0 + \rho')(\vec{V_0} + \vec{V'})) = 0 \tag{A.2}$$

Then,

$$\frac{\partial \rho_0}{\partial t} + \nabla \cdot (\rho_0 \vec{V_0}) + \frac{\partial \rho'}{\partial t} + \nabla \cdot (\rho_0 \vec{V'}) + \nabla \cdot (\rho' \vec{V_0}) + \nabla \cdot (\rho' \vec{V'}) = 0 \tag{A.3}$$

The mean flow already obeys conservation law, hence the first two terms are zero. Mean velocity field is assumed to be uniform, making fifth term zero. Also eliminating second order fluctuating term results in the linearised continuity equation :

$$\frac{\partial \rho'}{\partial t} + \rho_0 \nabla \cdot \vec{V'} = 0 \tag{A.4}$$

A.2 Momentum equation

The conservation of momentum in differential form without viscosity stresses and body forces can be described as,

$$\rho \frac{D\vec{V}}{Dt} + \nabla p = 0 \tag{A.5}$$

Linearise the gas properties around mean values,

$$(\rho_0 + \rho') \frac{D(\vec{V_0} + \vec{V'})}{Dt} + \nabla(p_0 + p') = 0 \tag{A.6}$$

Expanding,

$$\rho_0 \frac{\partial \vec{V_0}}{\partial t} + \rho_0 \vec{V} \cdot \nabla \vec{V_0} + \rho_0 \frac{\partial \vec{V'}}{\partial t} + \rho_0 \vec{V} \cdot \nabla \vec{V'} + \rho' \frac{\partial \vec{V_0}}{\partial t} + \rho' \vec{V} \cdot \nabla \vec{V_0} + \rho' \frac{\partial \vec{V'}}{\partial t} + \rho' \vec{V} \nabla \vec{V'} + \nabla(p_0 + p') = 0 \tag{A.7}$$

Assume $V_0 = 0$ as a special case of classical acoustics. And eliminate derivatives of uniform and constant terms p_0, ρ_0;

$$\rho_0 \frac{\partial \vec{V'}}{\partial t} + \rho_0 \vec{V'} \cdot \nabla \vec{V'} + \rho' \frac{\partial \vec{V'}}{\partial t} + \rho' \vec{V'} \cdot \nabla \vec{V'} + \nabla p' = 0 \tag{A.8}$$

Finally, by eliminating the second order fluctuations,

$$\rho_0 \frac{\partial \vec{V'}}{\partial t} + \nabla p' = 0 \tag{A.9}$$

gives the linearised momentum equation.

A.3 Energy Equation

The differential energy equation with a heat source term is simply known as,

$$\frac{\partial E_T}{\partial t} + \nabla \cdot \left[\vec{V}(E_T + p) \right] = Q \tag{A.10}$$

And it can be rewritten in per volume form as,

$$\frac{\partial \rho e_T}{\partial t} + \nabla \cdot \left[\vec{V}(\rho e_T + p) \right] = q \tag{A.11}$$

where $e_T = e + \frac{1}{2}|\vec{V}|^2$ is the total energy per mass and $e = C_v T$ is the internal energy per mass. It can be derived using ideal gas relations that,

$$p = \rho(\gamma - 1)e \tag{A.12}$$

Then,

$$\frac{\partial}{\partial t}\left(\rho\frac{p}{\rho(\gamma-1)} + \frac{1}{2}\rho|\vec{V}|^2\right) + \nabla\cdot\vec{V}\left(\rho\frac{p}{\rho(\gamma-1)} + \frac{1}{2}\rho|\vec{V}|^2 + p\right) = q \qquad (A.13)$$

Linearise the gas properties around mean values,

$$\frac{\partial}{\partial t}\left(\frac{p_0 + p'}{\gamma-1} + \frac{1}{2}(\rho_o + \rho')(\vec{V_0} + \vec{V'})^2\right)$$

$$+\nabla\cdot(\vec{V_0} + \vec{V'})\left(\frac{p_0 + p'}{\gamma-1} + \frac{1}{2}(\rho_0 + \rho')(\vec{V_0} + \vec{V'})^2 + p_0 + p'\right) = q \qquad (A.14)$$

As before, the mean velocity is assumed to be zero and mean pressure and density be uniform.

Also neglect second order fluctuating terms,

$$\frac{1}{\gamma-1}\frac{\partial p'}{\partial t} + \frac{p_0}{\gamma-1}\nabla\cdot\vec{V'} + p_0\nabla\vec{V'} = q \qquad (A.15)$$

After some manipulations linearised energy equation shows up,

$$\frac{\partial p'}{\partial t} + p_0\gamma\nabla\cdot\vec{V'} = (\gamma-1)q \qquad (A.16)$$

Appendix B

ANALYTICAL SOLUTION OF THE SIMPLE CASE

The following PDE is to be solved analytically

$$\frac{\partial^2 \hat{p}}{\partial x^2} + k^2 \hat{p} = 0$$

$$\text{with} \frac{\partial \hat{p}}{\partial x} = 0 \text{ at } x = 0$$

$$\text{and } \frac{\partial \hat{p}}{\partial x} - \frac{ik}{Z} \hat{p} = 0 \text{ at } x = L \tag{B.1}$$

To begin with, assume a general harmonic solution satisfying the equation with arbitrary coefficients in complex domain

$$\hat{p} = c_n^+ e^{ik_n x} + c_n^- e^{-ik_n x} \tag{B.2}$$

$$\frac{\partial \hat{p}}{\partial x} = c_n^+ ik_n e^{ik_n x} - c_n^- ik_n e^{-ik_n x} \tag{B.3}$$

And for the first boundary condition at $x = 0$

$$c_n^+ ik_n - c_n^- ik_n = 0$$

$$c_n^+ = c_n^- = c_n \tag{B.4}$$

For the second condition at $x = L$

$$c_n ik_n e^{ik_n L} - c_n ik_n e^{-ik_n L} - \frac{ik_n}{Z}(c_n e^{ik_n L} + c_n e^{-ik_n L}) = 0 \tag{B.5}$$

or,

$$e^{ik_n L} - e^{-ik_n L} = \frac{1}{Z}(e^{ik_n L} + e^{-ik_n L}) \tag{B.6}$$

and substituting trigonometric forms by Euler's formula

$$\frac{i sin k_n L}{cos k_n L} = \frac{1}{Z}$$

$$tan k_n L = \frac{-i}{Z} \tag{B.7}$$

equivalently,

$$tan(k_n L - n\pi) = \frac{-i}{Z}$$

(B.8)

Finally,

$$k_n = n\frac{\pi}{L} + \frac{1}{L}tan^{-1}\left(\frac{-i}{Z}\right)$$

(B.9)

is the general solution of the dispersion relation where $n \in N$.